CERES Edition-2 Cloud Property Retrievals Using TRMM VIRS and Terra and Aqua MODIS Data, Part II: Examples of Average Results and Comparisons with Other Data

Patrick Minnis, Szedung Sun-Mack, Yan Chen, Mandana M. Khaiyer, Yuhong Yi, J. Kirk Ayers, Ricky R. Brown, Xiquan Dong, Sharon C. Gibson, Patrick W. Heck, Bing Lin, Michele L. Nordeen, Louis Nguyen, Rabindra Palikonda, William L. Smith, Jr., Douglas A. Spangenberg, Qing Z. Trepte, Baike Xi

Abstract—Cloud properties were retrieved by applying the Clouds and Earth's Radiant Energy System (CERES) project Edition-2 algorithms to 3.5 years of Tropical Rainfall Measuring Mission Visible and Infrared Scanner data and 5.5 and 8 years of MODerate Resolution Imaging Spectroradiometer (MODIS) data from Aqua and Terra, respectively. The cloud products are consistent quantitatively from all three imagers; the greatest discrepancies occur over ice-covered surfaces. The retrieved cloud cover (~59%) is divided equally between liquid and ice clouds. Global mean cloud effective heights, optical depth, effective particle sizes, and water paths are 2.5 km, 9.9, 12.9 µm, and 80 gm^{-2}, respectively, for liquid clouds and 8.3 km, 12.7, 52.2 µm, and 230 gm^{-2} for ice clouds. Cloud droplet effective radius is greater over ocean than land and has a pronounced seasonal cycle over southern oceans. Comparisons with independent measurements from surface sites, the Ice Cloud and Land Elevation Satellite, and the Aqua Advanced Microwave Sounder-EOS are used to evaluate the results. The mean CERES and MODIS Atmosphere Science Team cloud properties have many similarities but exhibit large discrepancies in certain parameters due to differences in the algorithms and the number of unretrieved cloud pixels. Problem areas in the CERES algorithms are identified and discussed.

Index Terms— Climate, Cloud, cloud remote sensing, Clouds and the Earth's Radiant Energy System (CERES), Moderate Resolution Imaging Spectroradiometer (MODIS), Visible and Infrared Scanner (VIRS)

I. INTRODUCTION

Understanding the relationship between clouds and solar and longwave radiation processes requires determination of cloud property distributions and the radiation budget. The NASA Clouds and Earth's Radiant Energy System (CERES) Project [1] was designed to facilitate this understanding by measuring the top-of-atmosphere radiation fields simultaneously with cloud properties using instruments onboard several satellites to provide global and diurnal coverage. The CERES scanners measure broadband shortwave and combined (total) shortwave and longwave radiances on the Tropical Rainfall Measuring Mission (TRMM), *Terra* and *Aqua* satellites. The Visible Infrared Scanner (VIRS) on the TRMM [2] and the Moderate Resolution Imaging Spectroradiometer (MODIS) on *Terra* and *Aqua* [3] are used to discriminate between clear and cloudy scenes and to retrieve cloud and aerosol properties. Cloud properties, including cloud fraction, phase, temperature, height, optical depth, effective particle size, and condensed/frozen water path, are key parameters that link the atmospheric radiation and hydrological budgets. The CERES radiation measurements and their inversion as well as the methods for identifying cloudy pixels and retrieving aerosol properties in clear pixels have been described elsewhere [4]-[8]. A companion paper documents the CERES Edition-2 (Ed2) cloud property retrieval system (CPRS) algorithms, the raw input, and some of the history and motivation for retrievals [9]. This paper summarizes the Ed2 results to date for VIRS and MODIS data taken since 1998 and 2000, respectively. Comparisons with independent retrievals and measurements are also presented to place the CERES results in the context of another set of global retrievals and provide a sense of the accuracy of the products.

II. DATA

The cloud parameters considered here include cloud phase, effective temperature T_c, height z_c, and pressure p_c, cloud top height z_t or pressure p_t, optical depth τ, droplet effective radius r_e or ice crystal effective diameter D_e, and liquid LWP or ice IWP water path.

A. Satellite cloud properties

1) CERES Ed2 cloud retrievals: The CPRS Ed2 algorithms used to retrieve the cloud properties from TRMM VIRS and Terra and Aqua MODIS imagery are mentioned only briefly here because they are described in Part I [9]. During daytime, when the solar zenith angle (SZA) is less than 82°, the Visible Infrared Shortwave-infrared Split-window Technique (VISST) is used to retrieve cloud properties over snow-free surfaces. The Shortwave-infrared Infrared Near-infrared Technique (SINT) is used over snow and ice covered surfaces during the day. At all other times, the Shortwave-infrared Infrared Split-window Technique (SIST) is used. The VISST and SINT use the visible (0.65-µm) and near-infrared (NIR: 1.62 µm for Terra and 2.13 µm for Aqua), respectively, to retrieve τ, the infrared (10.8 µm) to retrieve the T_c, the shortwave-infrared (3.8 µm) to estimate r_e or D_e, and the split-window (12.0 µm) channel to aid in phase determination. The SIST uses the 3.8, 10.8, and 12.0-µm channels to retrieve the same parameters. LWP and IWP are computed from the product of τ and either r_e or D_e respectively. The parameters, Z_c, p_c, Z_t, and p_t are determined from T_c, a relevant sounding, and empirical parameterizations.

The CERES Ed2 cloud properties reported here are based on individual pixel retrieval values, Single Scanner Footprint (SSF) convolved average instantaneous properties, and 1° monthly averages computed from pixel-level results as part of the quality control process. The VIRS analyses used all of the 2-km VIRS pixels while the CPRS was only applied to every fourth MODIS 1-km pixel on every other scan line yielding an effective resolution ~2.8 km at nadir. Sampling and other characteristics of the analyzed data are discussed by [9].

Pixel-level results were retained for those imager granules (5-minute portions of the orbit) containing data located over a selected number of locations around the globe and also for one complete day of Terra MODIS orbits, 30 July 2005. VIRS monthly means were computed using imager data taken from January 1998 through July 2001. The VIRS analyses continued beyond March 2000 after the TRMM CERES scanners failed under a plan to produce pseudo-SSF data using narrowband to broadband conversions. The processing was stopped with July 2001 data because of project priorities. Terra and Aqua MODIS monthly means taken from the periods February 2000 through December 2007 and from July 2002 through December 2007, respectively, are considered here. Longer-term averages are computed from the monthly means. The CERES quality control cloud products are available at http://lposun.larc.nasa.gov/~cwg/. The CERES SSF data are available at the NASA Langley Atmospheric Science Data Center (http://eosweb.larc.nasa.gov/). After this paper was submitted, MODIS data taken between January 2008 and December 2010 were also analyzed.

2) MODIS Atmospheres Science Team (MAST) Collection 5: Pixel-level cloud properties are derived from MODIS data by the MODIS Atmosphere Science Team (MAST) with algorithms that use many of the 36 MODIS spectral bands [10] – [12] and auxiliary input data that often differ from the CERES input data. Updates to the original MAST algorithms, which have been used to generate the standard Collection-5 MAST products, i.e., Terra/Aqua MOD06/MYD06 and MOD35/MYD35 products, are described by [13] – [15]. The Terra MOD06 data are sampled in the same manner used by CERES to facilitate one-to-one instantaneous comparisons. The October MOD08/MYD08 monthly averages are used for more comprehensive comparisons with the CERES retrievals.

3) Advanced Microwave Scanning Radiometer – EOS (AMSR-E): The LWP values retrieved from VISST using Aqua MODIS data over ocean were matched with LWP retrievals from the Aqua AMSR-E during July 2004. The standard (EOS) AMSR-E LWP values were computed using the method of [16], while an alternative (Lin) set of values were computed using the method of Lin et al. [17]. These data are matched in the same manner used by [18]. Monthly mean LWP is first computed for each 1° region using only those non-precipitating AMSR-E footprints outside of sunglint-affected areas and having CERES liquid water cloud fractions greater than 98%. Zonal averages are computed from the regional values and finally global mean values are derived from the zonal means.

4) Ice Cloud and Land Elevation Satellite (ICESat): The ICESat Geoscience Laser Altimeter System (GLAS) cloud height and optical analyses are used to define cloud top heights and vertical structure through the atmosphere [19]. The medium resolution (5-Hz) V28 version of GLA09 Level 2 Global Cloud Heights Including Multiple Layers dataset is used to define the cloud boundaries through the atmosphere from top to bottom for all clouds having a cumulative $\tau < 3$ or so. Once the cumulative optical depth exceeds that threshold, the lidar beam penetrates no farther such that any clouds at lower altitudes are undetected and the base of the last detected layer is unknown. If the surface is detected, then a complete vertical profile of the clouds is obtained.

Exact temporal and spatial matching is ideal for comparing retrievals from two different spacecraft. However, *Terra* and *Aqua* have nominal equatorial crossing times of 1030 and 1330 LT, respectively, while during the GLAS laser period 2a, 25 September - 18 November 2003, the ICESat equatorial crossing times ranged from 0818/2018 on 25 September 2003 to 0655/1855 LT on 18 November 2003. While some collocations of the MODIS and GLAS data occur at high latitudes, few matches can be obtained in the Tropics. To obtain a global estimate for comparison with the CERES-MODIS cloud properties, it is necessary to use a statistical approach that compares average heights from GLAS for 2° x 2° regions with similar quantities derived from the CM pixel-level data for the 55-day period. Such comparisons can only be used to estimate the average biases in the CM data and provide no information about instantaneous errors.
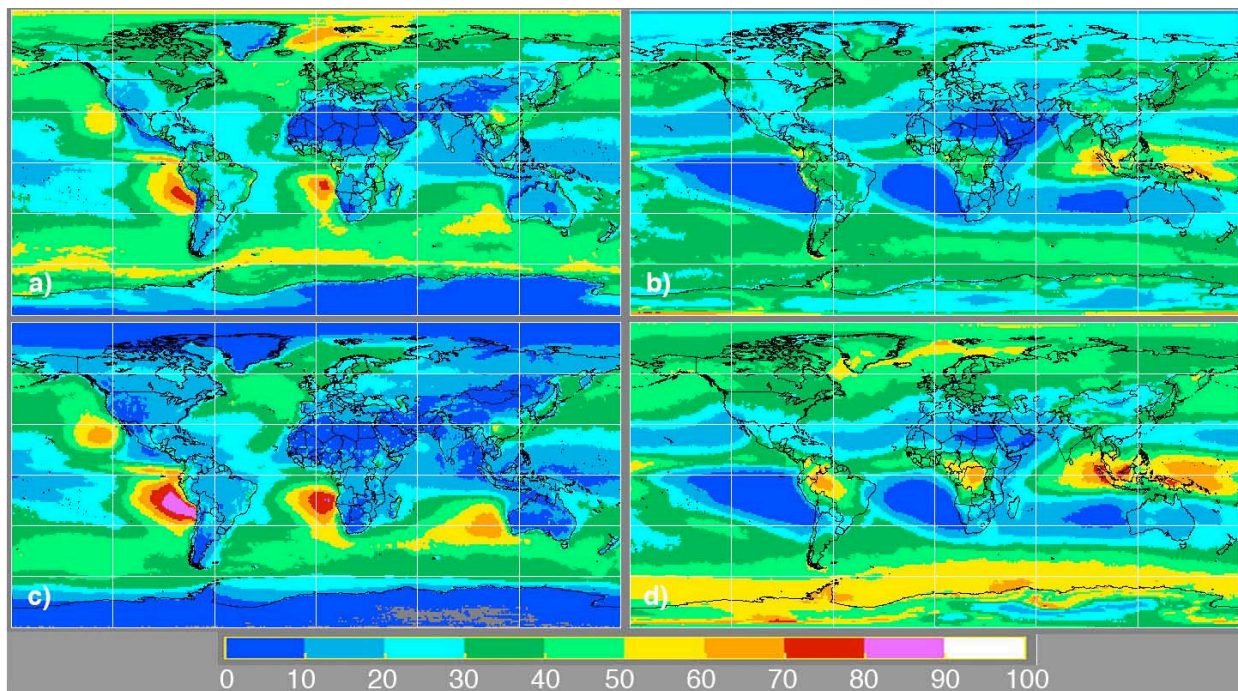
Fig. 1. Cloud fraction (%) by phase, Aqua, 2002-2007. (a) day liquid, (b) day ice, (c) night liquid, and (d) night ice.

B. Surface-based observations

Comparisons are performed between the CERES retrievals and data acquired for single-layer, overcast clouds using active and passive instruments from the Atmospheric Radiation Measurement (ARM) Program Southern Great Plains Central Facility (SCF; 36.6°N, 97.5°W) [20] and the ARM Mobile Facility (AMF) site at Pt. Reyes, CA (38.09°N, 122.96°W) [21]. At the SCF, cloud boundaries and microphysical products are taken from the ARM Mace PI Product (http://www.arm.gov/data/pi/19) [22]. The Mace products are based on lidar, ceilometer, and cloud radar measurements. The corresponding cloud top, base, and mean temperatures were determined from the nearest ARM rawinsonde temperature profiles. Cloud liquid water path was derived from the SCF microwave radiometer (MWR) brightness temperatures measured at 23.8 and 31.4 GHz using the method of Liljegren et al. [23]. For liquid water clouds, the LWP and uplooking broadband solar radiometer irradiances were used to retrieve τ and r_e following the approach summarized by Dong et al. [24]. The cirrus cloud microphysical properties, τ, IWP, and D_e, were determined using the Z-radiance method [25], [26] applied to Millimeter Cloud Radar (MMCR) and coincident Atmospheric Emitted Radiance Interferometer data. Averages of all microphysical properties were computed for the 1-h period centered on the satellite overpass time.

The AMF operated at Pt. Reyes from March through September 2005. Because the MMCR was not available, only LWP data based on the MWR radiances were used for the comparisons with CERES-MODIS retrievals. For a given Terra or Aqua overpass, a 15-min average of the MWR LWPs is matched with the LWP from the CERES SSF nearest the AMF site. Only SSF data having cloud fractions > 85%, T_c > 273.15 K, SZA < 80°, and viewing zenith angles (VZA) $\leq$ 60° were matched with MWR data having at least 30 2-s observations, no precipitation or quality control flags, and LWP > -40 gm^{-2}.

III. Result Examples

CERES Ed2 cloud property averages are listed in Table I for three domains. It should be noted that all retrievals assume that the clouds in a given pixel are all in one layer so that ice clouds above liquid clouds will most often obscure the underlying clouds and the properties will be computed assuming the clouds in the column are composed entirely of ice. Thus, properties of both ice and liquid clouds are impacted by these multilayer effects.

Mean cloud fraction is plotted according to pixel phase in Fig. 1 for Aqua. During daytime (Fig. 1a), liquid clouds are most common in the marine stratocumulus regimes, over south central China, in the southern midlatitudes, and northwest of Scandanavia. At night (Fig. 1c), the Arctic and southern midlatitude maxima disappear and liquid cloud cover, in general, is significantly reduced over many land areas, while the marine stratus peaks are reinforced. Daytime ice clouds (Fig. 1b) are most common over the maritime continent and infrequently detected over the Sahara and Saudi Arabian Deserts, and the southern marine stratus regions. At night, the ice cloud fraction is substantially increased over the polar regions, many land areas, and the southern midlatitudes (Fig. 1d). The actual liquid cloud fraction in areas where ice clouds are common is likely to be greater because of the occurrence of multilayered cloud systems that are interpreted as being ice clouds only. Both Terra and Aqua yield similar coverage by ice and water clouds when averaged for all times of day (Table I). The greatest differences are for ice clouds. Terra retrieves 0.016 more in the polar regions, while Aqua finds 0.011 more in non-polar areas. Unfortunately, no properties could be retrieved for 5.6% (4.9%) of the Terra (Aqua) cloudy pixels

during daytime and only 0.5% at night. Of all the daytime cloudy pixels in polar regions, 10% are no-retrievals compared to 3.9% in non-polar regions. In the latter domain, no-retrievals occur 9.7% of the time over land compared to only 2.0% over water. This surface-dependence of no-retrievals is a reflection of the uncertainties in clear-sky albedos and surface temperatures. The land no-retrievals occur most frequently over coastal deserts and the Tibetan Plateau, and along the boundaries of very bright (e.g., deserts) and dark (tropical forest) areas.

The day-night change in cloud phase is due to a variety of factors. In the polar regions, nighttime primarily occurs during the hemispheric winter when temperatures are mostly too cold for liquid water clouds. In the Tropics, the cirrus generated by late evening thunderstorms is likely to persist and obscure lower clouds. Algorithm differences also contribute to the apparent change in phase fraction. The lack of information in the infrared channels for optically thick clouds make phase selection difficult for the SIST in the supercooled temperature range, especially for $82° < SZA < 90°$. Because the SIST uses the threshold of 253 K to select phase for optically thick clouds at night, many supercooled liquid clouds with $T_c < 253$ K are misclassified as ice clouds. During the daytime, 10.9% of the liquid cloud pixels have $T_c < 253$ K compared to only 1.0% at night. These cold liquid clouds are most likely to occur in the midlatitudes and, hence, the switch from liquid to ice cloud maxima in these areas may be due, in large part, to that algorithm artifact. Another feature of the SIST is that it is relatively insensitive to the background temperature, so that, in situations having thin cirrus over a low cloud, the SIST often retrieves the high cloud, which is missed during the daytime. When the low cloud has a temperature similar to the underlying surface, the SIST will tend to interpret the overlapped scene as a thin ice cloud if the brightness temperature difference between the 10.8 and 12.0 μm channels is significantly greater than zero. At night, there will be an increase in the number of overlapped clouds identified as ice and a reduction in those interpreted as liquid water. Thus, at least, two algorithmic effects cause an apparent increase in ice clouds at night over the Tropics and continental areas.

The long-term mean values of Z_c in Fig. 2 show some significant day-night differences. Over ocean (Fig. 2a) and many land areas (Fig. 2b) between 50°S – 50°N, Z_c for liquid water clouds tends to increase at night, especially where convection is common. In the southern midlatitudes, Z_c drops at night, probably as a result of the increase in pixels identified as ice clouds (Fig. 15). Ice cloud heights (Fig. 2c,d) increase over most areas at night, perhaps, because of the daytime convection, but mostly because Z_c retrieved by the SIST is closer to the cloud top than that from VISST [24]. The mean cloud heights for all Terra samples (Fig. 2e) appear to be slightly less than those from Aqua (Fig. 2f), especially for areas dominated by high clouds. Figure 2g shows the mean daytime differences, Aqua – Terra (A –T), and the standard deviations, σ(A-T), of the monthly mean differences. The daytime differences represent the average change in the 3 h between the 1030-LT Terra and 1330-LT Aqua orbits. The

greatest positive changes in non-polar areas occur along tropical coastlines and over mountain ranges and plateaus, while the negative changes are most intense in lowlands. These differences are most likely due to the diurnal cycle in convection. The standard deviations (Fig. 2h) are greatest where diurnal difference is primarily a seasonal phenomenon. The relatively large positive differences over the polar regions are primarily due to the algorithmic differences between the Aqua and Terra algorithms over snow [9]. When averaged over all areas and times, there is essentially no difference in the Aqua and Terra cloud heights (Table I).

The annual mean daytime cloud optical depths for both satellites are presented in Fig. 3. Liquid cloud optical depths (Fig. 3a, b) are greatest (between 16 and 32) over the midlatitudes, particularly over land. The peak values occur over southeastern China in the Aqua results (Fig. 3b). Over marine stratus areas, the largest values are retrieved from Terra (Fig. 3a), reflecting the diurnal cycle of those boundary layer clouds. The greatest difference occurs off the coasts of Chile and Peru (Fig. 3g). The small standard deviations of the differences (Fig. 12h) over marine stratus indicate that the morning-to-afternoon change occurs during all seasons. The Terra liquid and ice (Fig. 3c) cloud optical depths between 45°S and 70°S are also greater than those from Aqua (Fig. 3b,d), suggesting that those clouds also thin out during the daytime. Over land areas, τ from Aqua tends to be slightly greater than that from Terra, except over many flatland areas (Fig. 3g). The greatest positive values tend to track their Z_c counterparts (Fig. 2g). Over polar regions, the Aqua values are typically much less than those from Terra for liquid, ice, and all (Figs. 3e,f) clouds. Most of this difference is an artifact due to limitations of the 2.1-μm channel for τ retrievals and the mistaken use of the 1.6-μm atmospheric absorption values instead of those for 2.1 μm in the SINT. Overall, for areas covered by snow and ice, τ from Terra is approximately double the value from Aqua. In other areas, the differences in τ from the two satellites are quite small (Table I).

The mean seasonal distributions of r_e from Aqua are plotted in Figs. 4a-d, along with the 2002-2007 Aqua (Fig. 4e) and 2000-2007 Terra (Fig. 4f) annual means, and the mean differences (Fig. 4g) and standard deviations of the monthly differences (Fig. 4h). The effective droplet sizes over land are significantly smaller than those over marine areas with the largest continental values occurring over the Amazon and Congo River basins. Large values are also retrieved over Siberia and Greenland during winter (Fig. 4a), but they are concurrent with large SZAs and small optical depths (τ < 4, not shown) over snow and are, thus, highly uncertain. The smallest r_e values occur over some desert areas and could be due to an excessive number of cloud condensation nuclei, dust mistaken as clouds, or both. There is little seasonal variation in r_e over Saudi Arabia and the Sahara. Over the Northern Hemisphere oceans, the largest values of r_e occur during autumn (Fig. 4d) and winter with a minimum during spring (Fig. 4b). Over the Southern Hemisphere, the maximum values occur during the austral winter (Fig. 4c) and are
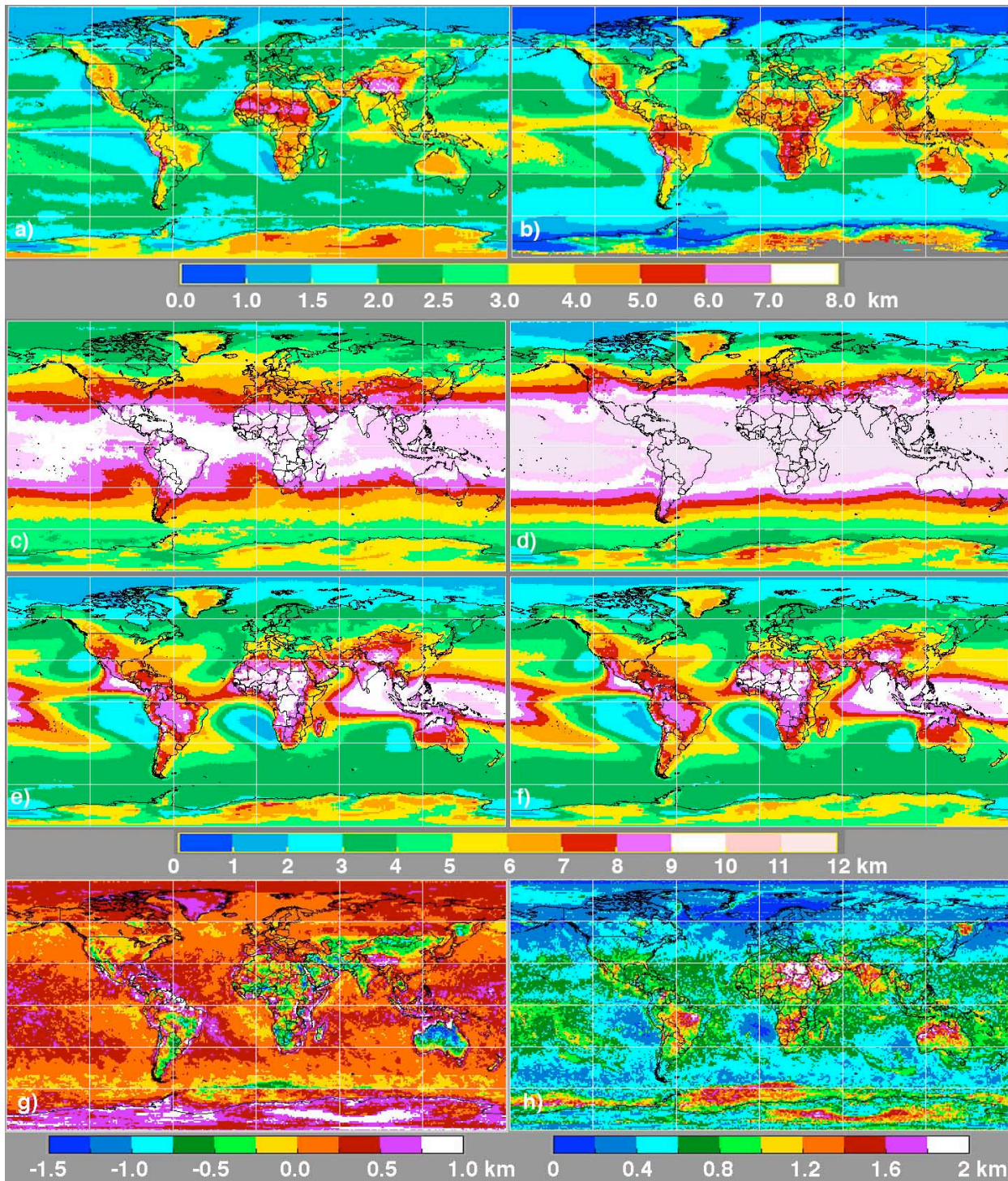
Fig. 2. CERES mean cloud effective heights: (a-e) Terra 2000-2007, (f) Aqua 2002-2007, and (g,h) Terra-Aqua height differences. (a) day, liquid clouds, (b) night, liquid clouds, (c) day, ice clouds, (d) night, ice clouds, (e, f) total cloud cover day + night; (g) day total cloud height differences and their (h) monthly standard deviations for 2002-2007.

substantially larger than the maximum values found north of the Equator. The mean annual distributions of r_e from Aqua (Fig. 4e) and Terra (Fig. 4f) are very similar except that the Terra values are 0.4-µm smaller than their Aqua counterparts (Table I). If there were no differences due the sampled times of day, an Aqua – Terra r_e difference of ~0.5 µm would be expected because of the 0.55 K difference between the Terra and Aqua 3.8-µm brightness temperatures [5] that are used to diagnose r_e. Differences between 0 and 1 µm in Fig. 4g are not

likely to be significant. The afternoon decrease in r_e off the coasts of Peru and Chile and the increases over the Amazon, central Africa, and the maritime continent are probably significant. The larger differences over Mongolia and other high-latitude areas are most likely due to differences in the Aqua and Terra processing over snow. The largest standard deviations (Fig. 4h) mostly occur over bright surfaces where clouds are scarce or snow is seasonal. The VIRS retrievals of τ and r_e are reasonably consistent with the Terra results as

TABLE I
ANNUAL MEAN CLOUD PARAMETERS DERIVED FROM MODIS USING THE CERES CPRS. TERRA, 2000-2007; AQUA, 2002-2007.

Parameter	Global (90°S – 90°N)		Non-Polar (60°S – 60°N)		Polar (60°N-90°N, 60°S – 90°S)	
	Terra	Aqua	Terra	Aqua	Terra	Aqua
Liquid cloud fraction	0.293	0.287	0.304	0.296	0.226	0.232
Ice cloud fraction	0.293	0.301	0.274	0.285	0.417	0.401
No-retrieval fraction, day	0.036	0.031	0.023	0.024	0.118	0.073
Liquid cloud Z_c (km)	2.63	2.44	2.72	2.50	2.07	2.03
Ice cloud Z_c (km)	8.31	8.29	8.94	8.90	4.24	4.37
All cloud Z_c (km)	5.38	5.35	5.67	5.64	3.47	3.50
Liquid cloud τ, day	10.2	9.6	9.6	9.4	13.8	11.3
Ice cloud τ, day	12.9	12.6	13.6	13.6	8.6	6.5
r_e (µm), day	12.7	13.1	12.9	13.3	11.4	11.8
D_e (µm), day	53.5	50.5	52.9	50.5	56.3	50.7
LWP (gm^{-2}), day	81.3	78.6	78.5	78.2	99.7	81.1
IWP (gm^{-2}), day	239.3	221.3	255.2	239.8	136.6	101.8

shown in Fig. 5, which plots the daytime averages for the year, 2000. In general, the distribution of r_e from VIRS is very similar to that from Terra even though the mean value is ~1-µm larger than its Terra counterpart, due in part to the 0.55 K difference between the Terra and VIRS 3.8-µm brightness temperatures [5] and possibly to diurnal variations not captured by Terra. Figure 6 shows the seasonal zonal means of r_e over ocean retrieved from Terra MODIS for 2000-2003 (Fig. 6a) and compares them to their VIRS counterparts from 1998-2001 (Fig. 6b). As indicated by Fig. 4 also, r_e in the Southern Hemisphere is greatest during the coldest season (JJA) and smallest during austral summer (DJF), varying by 3-4 µm between 30°S and 60°S. In contrast, the mean r_e changes by only ~1-2 µm over the annual cycle in the Northern Hemisphere between 40°N and 60°N with the smallest values occurring during spring. For their common latitudes, both datasets are quite consistent (Fig. 6b). Because VIRS measures at all times of day over a 46-day period, it samples all available SZAs at a given location and, therefore, it is unlikely that SZA changes are responsible for the seasonal variations in the Terra results. The hemispherical discrepancies could be due to differences in the numbers of cloud condensation nuclei as a result of greater land coverage and more anthropogenic sources in the Northern Hemisphere. The mean daytime values of D_e in Fig. 7 show significant land-ocean differences and discrepancies between Aqua and Terra. On average, D_e from Aqua is 2.4-µm smaller than that from Terra in non-polar regions (Table I). This difference is evident when comparing Figs. 7a and 7b. Yet, over land, the mean D_e from Aqua is 45.9 µm, 0.6-µm greater than its Terra counterpart. The non-polar land-ocean difference is 10.2 µm for Terra compared to only 6.2 µm for Aqua. The differences are likely due to diurnal changes, calibration differences, and, over the polar regions, the differences in optical depths arising from the use of different spectral channels. As seen in Fig. 7g, the A-T differences in polar regions are mostly < -4 µm reflecting the algorithmic differences over snow and ice. The

positive differences over many of the ocean areas are not particularly significant given the large standard deviations (Fig. 7d) and small ice cloud fractions in those areas (Fig. 2b). However, over many land areas, the larger positive differences reflect the increase in ice cloud cover, τ, and mean Z_c discussed earlier likely due to diurnally dependent convective cycles.

Retrievals of cloud optical properties are much less reliable at night than during the day because of the limited information for $\tau > 3$ or 4 and the sensitivity of the cloud particle size retrievals to small errors in τ, surface emissivity ε_s, and surface skin temperature [9]. Nevertheless, the SIST retrieves patterns in mean τ (Fig. 8a) and r_e (Fig. 8b) over non-polar ocean areas at night that are comparable to their daytime counterparts (Figs. 3a and 4f). The maximum r_e values over oceans mostly occur in the same areas, while the minima in τ seem to be well correlated. Since the SIST constrains the optical depths, any variations in τ and r_e are due to clouds having $\tau < 8$ and, in some instances, $\tau < 32$ (see Fig. 11 in [9]). There is less apparent correlation between day and night retrievals over land, especially over deserts. The large spatial and spectral variability in ε_s may be the primary source of the biases. The nocturnal retrievals of D_e (not shown) appear to have no correlation with their daytime counterparts. As noted in Part I [9], the nighttime microphysical property retrievals were intended primarily to adjust the heights of optically thin clouds and not necessarily to retrieve accurate values of particle size. It is encouraging that the SIST is providing some information about r_e at night for optically thin clouds. Perhaps, refinement of the algorithm could yield reliable data about D_e at night also. The average daytime cloud liquid water paths are plotted in Fig. 9 for both satellites along with the Aqua – Terra differences and their monthly mean standard deviations. Aqua has smaller mean LWP than Terra over the marine stratus regions off the subtropical west coasts of Australia, Africa, and the Americas with the greatest difference off the coasts of
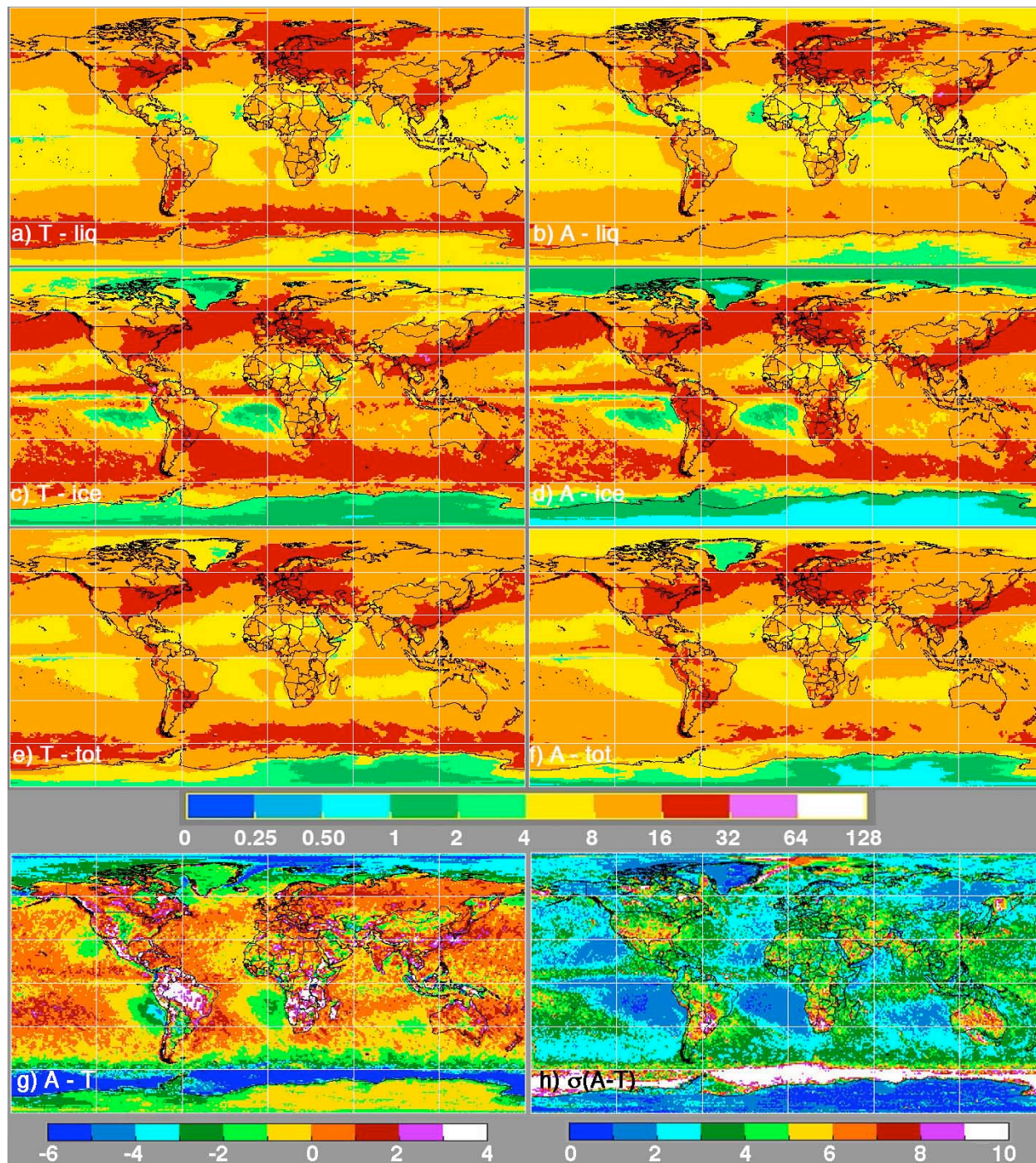
Fig. 3. Mean daytime cloud optical depths, Terra (T) 2000-2007 (a, c, e) and Aqua (A) 2002-2007 (b, d, f). Mean (g) total cloud optical depth differences and (h) their monthly standard deviations for 2002-2007.

Peru and Chile. The standard deviations (Fig. 9d) are smallest over southern marine stratus areas indicating a very small seasonal component in the diurnal changes. The difference is reversed near the Equator and over mid-ocean areas in the tropical convergence areas. In the midlatitudes, Aqua tends to have lower LWP values than Terra, especially in the Southern Hemisphere. Part of the difference may be due to Aqua classifying more thick clouds as ice or to actual thinning of the water clouds during the day. Over land, the differences between the satellites are mixed. Large positive differences occur over Central America, the Amazon Basin, Indonesia,

and eastern China. The greatest negative values occur over western North America, Africa, Australia, and Tibet. Overall, the mean LWP is the same for both satellites in non-polar regions (Table I). Maps of the mean IWP distributions have already been shown by [27], so Fig. 10 compares the zonal daytime means from Terra and Aqua and shows the distributions of the Aqua – Terra differences and their monthly mean standard deviations. On average, total IWP (Fig. 10a) from Terra exceeds that from Aqua, especially in the southern midlatitudes, where LWP is also smaller. Exceptions to this generalization are found at 15°S and between 50°N and 70°N.
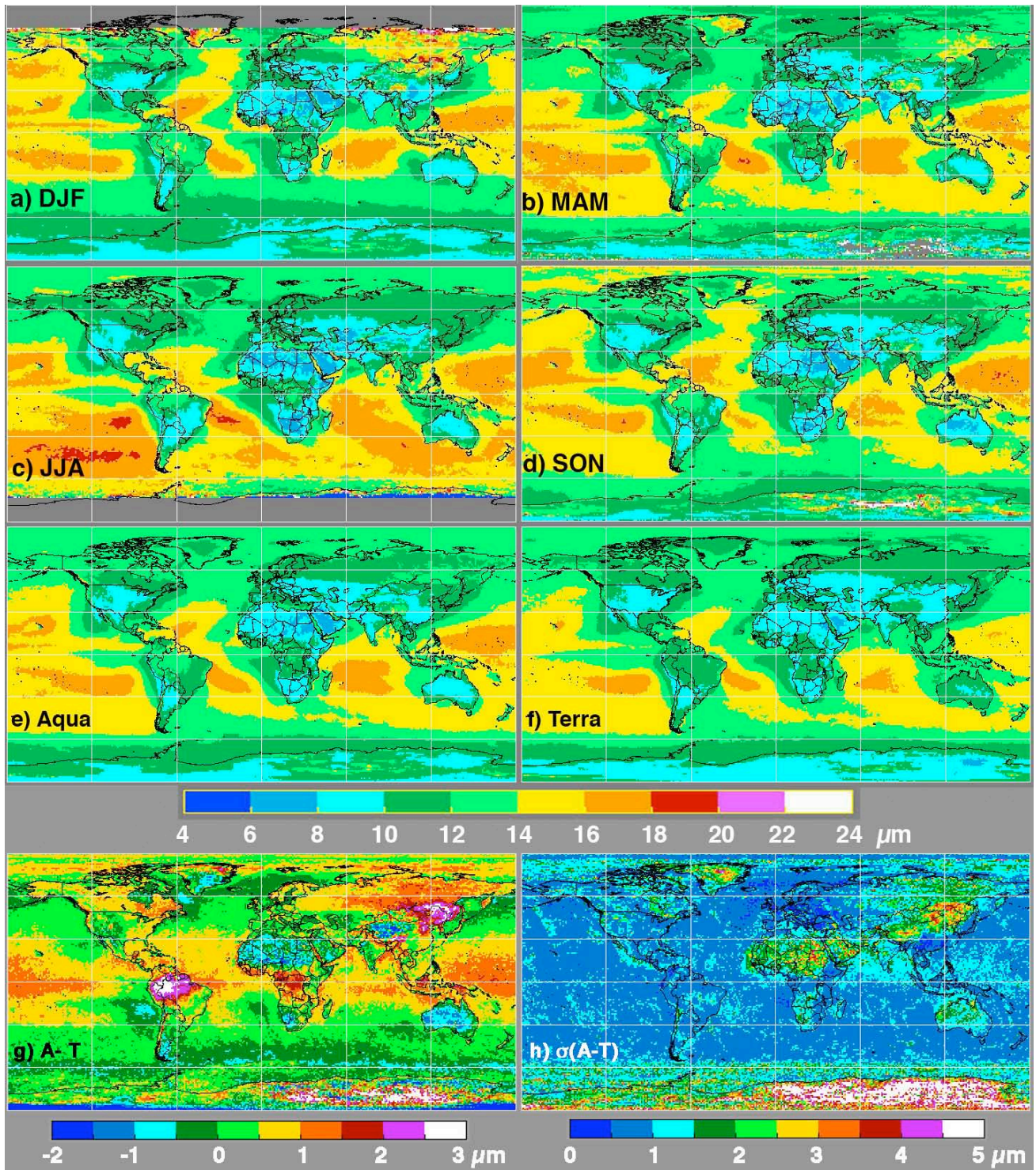
Fig. 4. Mean daytime cloud droplet effective radius, Aqua 2002-2007 (a-e), Terra 2000-2007 annual (f). Winter – DJF, Spring – MAM, Summer – JJA, Autumn – SON. Mean (g) differences and (h) their monthly standard deviations for 2002-2007.

For the latter area, the seasonal variations (Fig. 10e) and algorithmic changes are most likely responsible for the differences, while in the former zone the deep convection over land compensates for the average decreases over ocean (Fig. 10d). Over ocean (Fig. 10b), IWP from Terra exceeds that from Aqua in every zone, on average, most likely because of Aqua's reduced value of D_e. Except for a few areas over land, IWP from Aqua exceeds that from Terra, especially in the Southern Hemisphere (Figs. 10c,d). Overall, the Terra IWP is

~15 gm^{-2} (6%) greater than its Aqua counterpart over non-polar regions (Table I). These extrapolar differences likely reflect a real diurnal (1030 LT vs. 1330 LT) change in ice cloud properties. Given the calibration differences [5], [28], the Aqua values should be greater than those from Terra if there were no diurnal changes. Moreover, since the average LWP from Aqua is less than that from Terra in the southern midlatitudes, it is apparent that the clouds, in general, tend to thin out during the afternoon in that part of the globe.
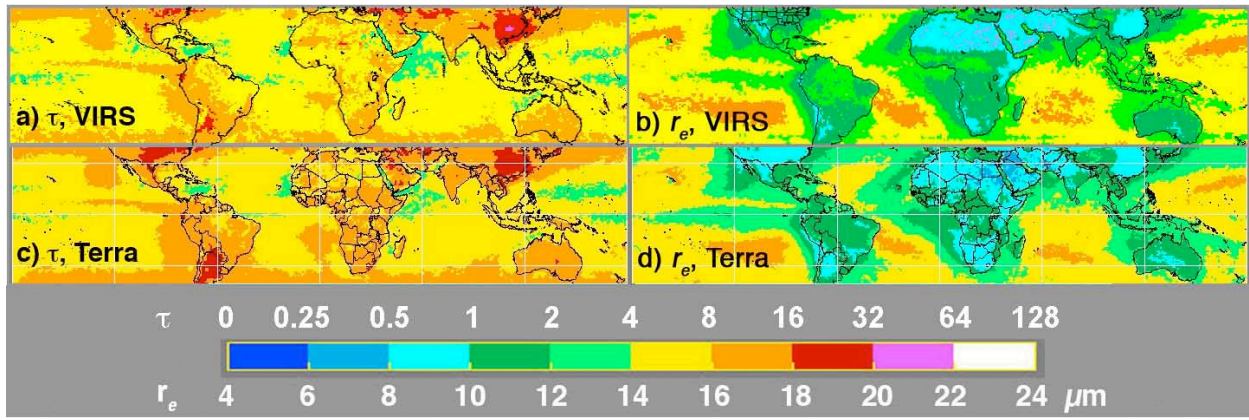
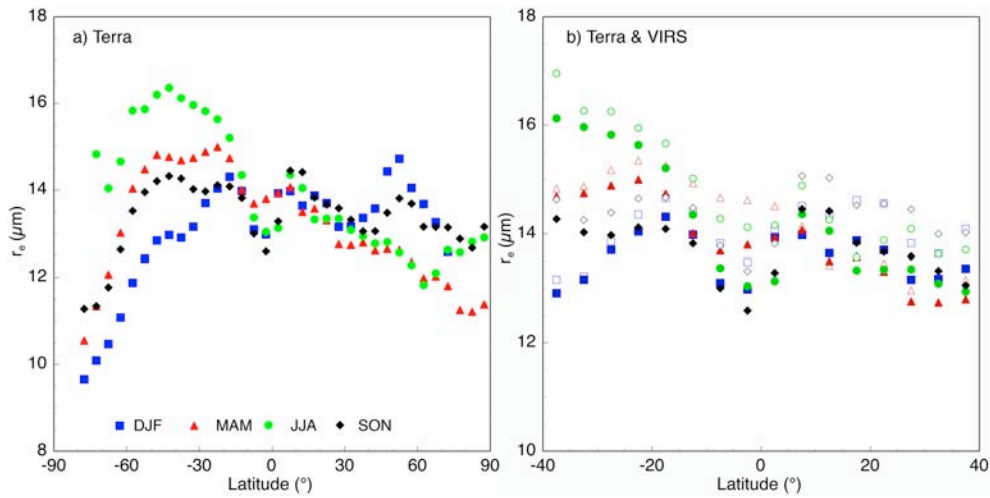Fig. 5. Mean cloud optical depths and effective droplet radii, 2000.

Fig. 6. Average seasonal maritime cloud effective droplet radii from Terra MODIS, 2000-2003 (solid symbols) and TRMM VIRS, 1998-2001 (open symbols). Seasons defined as in Fig. 4. Note scale difference between (a) and (b).
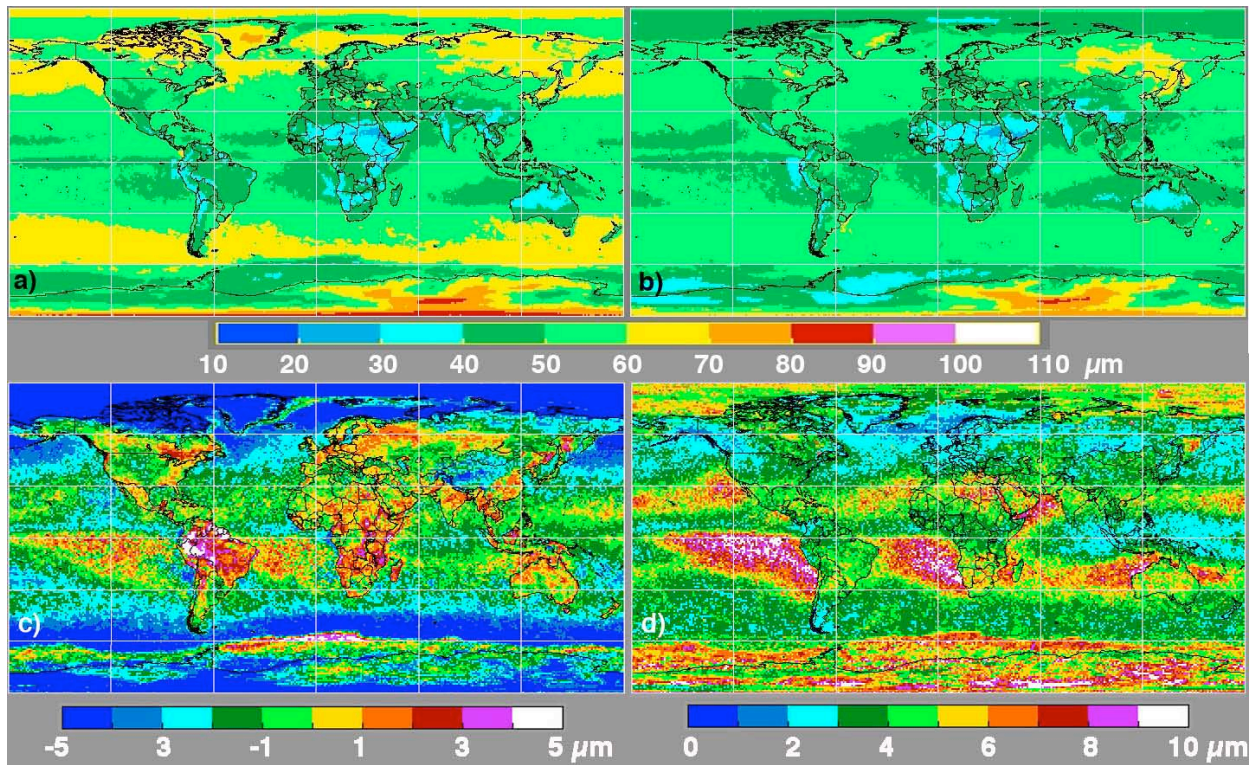

Fig. 7. Mean daytime cloud ice crystal effective diameter for (a) Terra, 2000-2007 and (b) Aqua, 2002-2007; and the (c) mean differences, Aqua – Terra, and (d) their monthly standard deviations for 2002-2007.
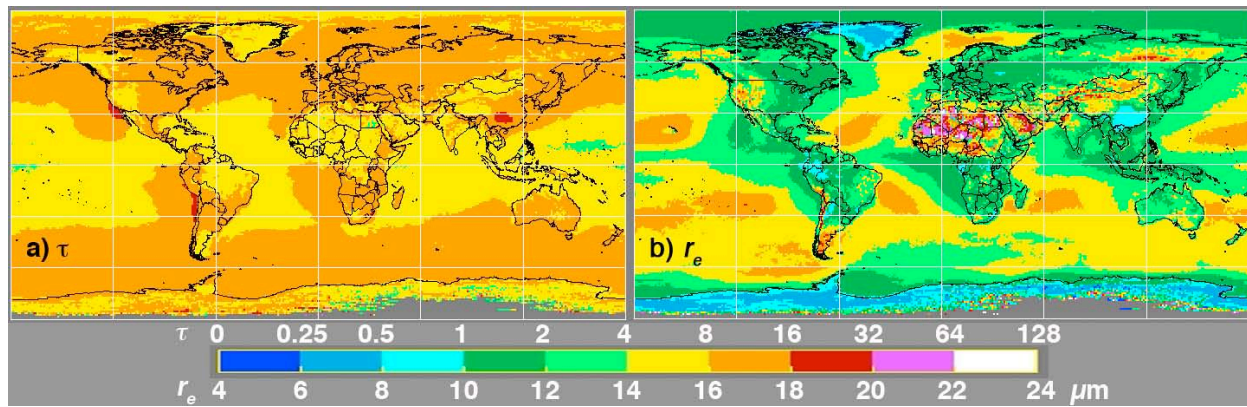
Fig. 8. Mean nighttime liquid cloud (a) optical depth and (b) droplet effective radius, Terra 2000-2007.

IV. KNOWN PROBLEMS AND COMPARISONS WITH INDEPENDENT DATA

The retrieval methods are subject to errors from many sources. The theoretical instantaneous uncertainties in effective particle size and τ are estimated to be on the order of 15% [24], however, these values only reflect the ideal situation for plane-parallel clouds. Clouds generally have structure that causes radiance anisotropies that are not taken into account by the plane-parallel cloud retrieval parameterizations. Comparisons of the retrievals with independent reference measurements provide a more realistic approximation of the uncertainties in the retrieved properties. Such comparisons have been performed using both the CERES-MODIS results and retrievals from other imagers, such as the AVHRR and the Geostationary Operational Environmental Satellites (GOES), using the CERES CPRS.

Uncertainties in the CERES cloud coverage have been discussed elsewhere [5]. Comparisons with the retrieved cloud parameters are discussed here. Table II provides a summary of the previous comparisons discussed in this section.

A. Cloud Heights

1) Low and midlevel clouds: CPRS-retrieved cloud effective and top heights have been compared for single-layer water clouds over land at the ARM SCF using surface-based radars and lidar and over water from satellite-borne lidars. For overcast stratus decks at the SCF, the CERES-MODIS effective cloud heights were ~0.6 $\pm$ 0.6 km below the radar-observed cloud top [24]. Approximately 0.1 km of the bias in that study could be due to the difference between the physical and radiating top of the cloud that is not taken into account for most liquid water clouds in the CPRS. A more extensive study using Z_t from GOES data over the SCF found that for clouds
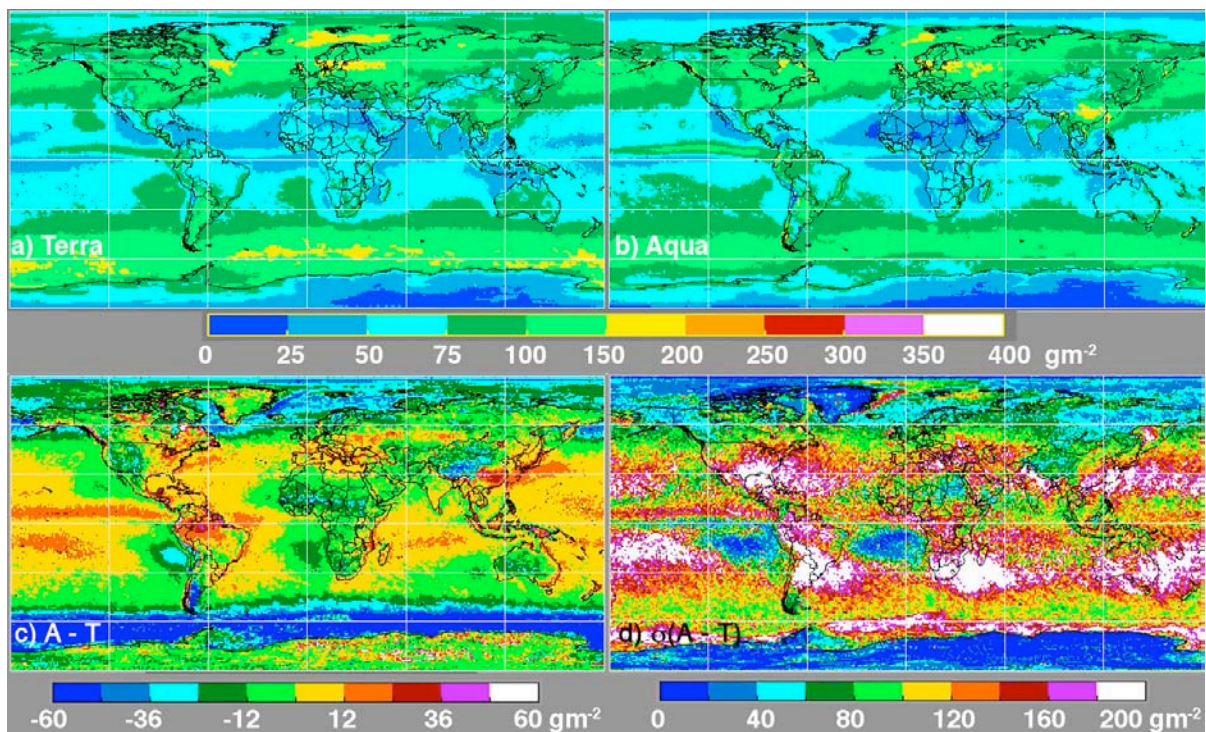

Fig. 9. Mean daytime cloud liquid water paths for (a) Terra, 2000-2007 and (b) Aqua, 2002-2007 with average (c) differences and (d) their monthly standard deviations for 2002 -2007.
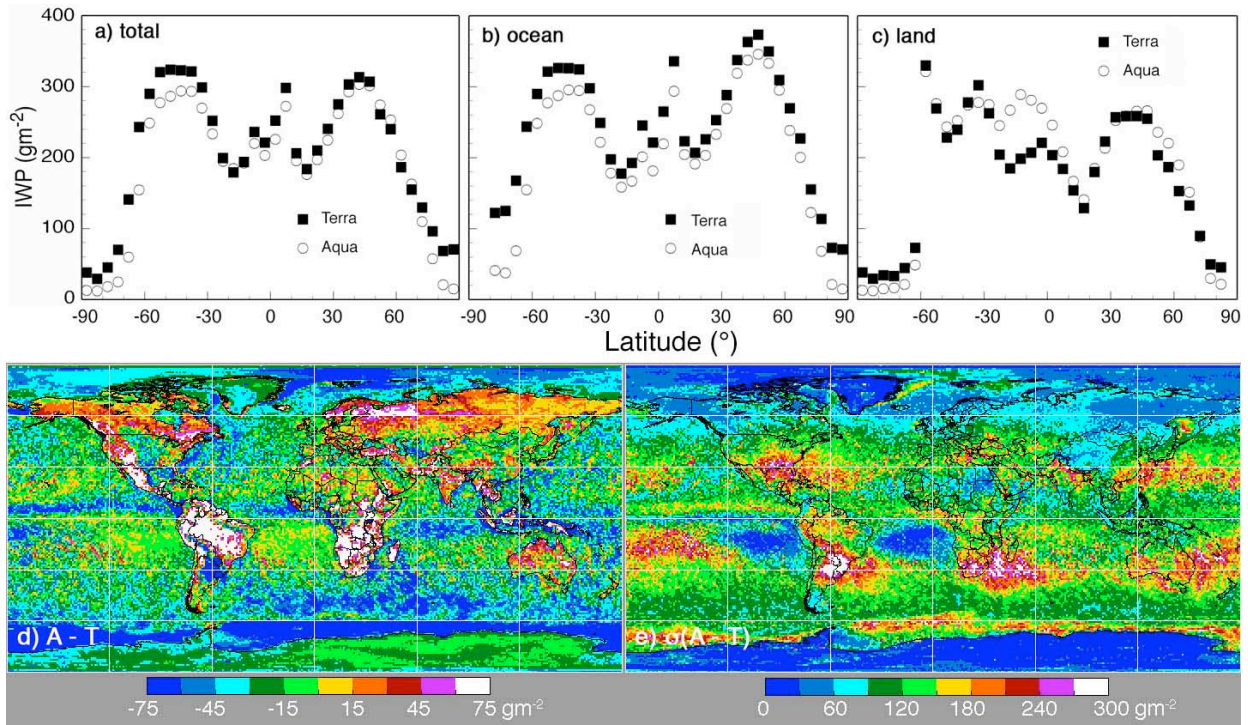
Fig. 10. Zonal mean ice water paths for Terra (2000-2007) and Aqua (2002-2007) with regional (d) differences and their (e) monthly standard deviations for 2002 -2007.

below 3 km, the cloud-top height underestimate was only ~0.15 ± 1.1 km with better precision during the day than at night [29]. That same study found that midlevel cloud heights were underestimated, on average, by 0.8 km during the day and by 1.1. km at night (Table II).

A preliminary global comparison using 1 month of single-layer cloud heights derived from Aqua MODIS data and from the Cloud-Aerosol Lidar and Infrared Pathfinder Satellite Observations (CALIPSO) found that for single-layer cloud tops below 3 km, the zonal mean Z_t is typically within ±0.5 km of the lidar-determined cloud tops over ocean [30]. Over land, Z_t underestimates the top height by ~0.5 km. For midlevel clouds, Z_t -Z_t(CALIPSO) averages between -0.2 in the tropics to -1.5 km over the southern polar regions.

2) High clouds: For 9 matches with Terra over the SCF having a mean τ of ~1.3, the average difference between the radar-determined cirrus cloud-top height and Z_c is 2.5 km [26]. Using GOES data, Smith et al. [29] found that Z_t from VISST was 1.9 ±1.7 km less than the cloud-top height found over the SCF, but was only 0.1 ±1.2 km less when using SIST. For optically thick ice clouds, the differences were 1.1 ± 1.1 km and 0.4 ± 0.7 km for VISST and SIST, respectively. Those differences are due to the assumption that $T_t = T_c − 0.5$ K, which has been shown to be an unusual occurrence [31].

Preliminary global comparisons of CALIPSO and CERES-MODIS single-layer high-cloud top heights [30] reveal underestimates by CERES that generally range from 1.5 to 3.5 km, while extreme differences of up to 8 km were found for the thinnest, highest clouds in the tropics. A more focused study also using CALIPSO data [32] found that the difference between Z_t and Z_t(CALIPSO) for optically thick ice clouds is typically 1- 2 km due to small values of ice water content

(IWC) in the tops of those clouds. The assumption in Ed2 that $Z_t < Z_c + 0.33$ km for optically thick ice clouds leads to biases in Z_t for those clouds. Thus, the top height is underestimated significantly for both thin and thick ice clouds.

Figure 11 presents scatterplots of the matched CERES-MODIS effective heights and ARM radar-derived cloud base Z_{Rb} and top heights Z_{Rt} and their corresponding temperatures for overcast, single-layer, optically thin (τ < 3) cirrus clouds over the SCF for Terra and Aqua data taken between March 2000 and December 2002. For the 17 daytime cases, Z_c is always lower than Z_{Rt}, but not always above Z_{Rb} (Fig. 11a). If the retrievals were always realistic, then Z_c would always be between Z_{Rt} and Z_{Rb}. On average, the differences, Z_c - Z_{Rb} and Z_c - Z_{Rt} are 0.6 and -2.6 km, respectively. These results are consistent with the studies noted earlier, but reveal that roughly two thirds of the Z_c values are reasonable in that they fall somewhere within the cloud, closer to the bottom than to the top. The effective radiating height for optically thin cirrus clouds varies depending on the vertical profile of IWC and temperature within the cloud. Because cirrus clouds tend to be bottom heavy in terms of IWC, the radiating temperature should typically be closer to the base than to the top depending on the cloud optical thickness. Nevertheless, it is clear that Z_c underestimates the cirrus cloud physical top during the daytime.

The corresponding cloud temperatures (Fig. 11b) behave in a similar manner, but with the opposite relationships. This indicates that the one-third of the cases having $Z_c < Z_{Rb}$ arise because of errors in the VISST retrieval and are not due to errors in the temperature profiles. Part of the bias in these and, perhaps, the other cases is due to the ozone absorption overestimate in the Ed2 VISST retrievals [9], which is greatest

TABLE II.
SUMMARY OF PREVIOUS COMPARISONS OF RETRIEVALS USING VISST/SIST WITH INDEPENDENT MEASUREMENTS, X.

Parameter	Independent measurement, X	VISST – X	σ	Number of samples	Satellite, [reference]
single-layer cloud heights		*(km)*	*(km)*		
low, day & night	radar, SFC	-0.6	0.6	178	MODIS, [24]
low, day	ARSCL, SFC	-0.1	0.7	458	GOES, [29]
low, night	ARSCL, SFC	-0.2	1.5	108	GOES, [29]
low, day & night	CALIPSO, global	-0.5 to 0.5	NA	$> 10^6$	MODIS, [30]
midlevel, day	ARSCL, SFC	-0.8	0.9	242	GOES, [29]
midlevel, night	ARSCL, SFC	-1.1	1.2	207	GOES, [29]
midlevel, day & night	CALIPSO, global	-0.2 to -1.5	NA	$> 10^6$	MODIS, [30]
high, day, $\tau < 3$	radar, SFC	-2.5	1.1	9	MODIS, [26]
high, day, $\tau < 3$	ARSCL, SFC	-1.9	1.7	173	GOES, [29]
high, day, $\tau \geq 3$	ARSCL, SFC	-1.1	1.1	539	GOES, [29]
high, night, $\tau < 3$	ARSCL, SFC	-0.1	1.2	301	GOES, [29]
high, night, $\tau \geq 3$	ARSCL, SFC	-0.6	0.9	584	GOES, [29]
high, day & night, $\tau > 8$	CALIPSO, global	-1.6	1.3	15,367	MODIS, [32]
high, day & night	CALIPSO, global	-2.0 to –3.0	NA	$> 10^6$	MODIS, [30]
optical depth		*%*	*%*		
liquid stratus	radar/radiometer, SFC	-5.8	40	72	GOES, [39]
liquid stratus	radar/radiometer, SFC	0.2	25	54	MODIS, [24]
cirrus	radiometer, SFC	29	58	47	GOES, [49]
cirrus	radar/radiometer, SFC	13	47	6	GOES, [25]
cirrus	radar, SFC	15	49	9	MODIS, [26]
particle effective size		*μm*	*μm*		
liquid stratus	radar/radiometer, SFC	1.4	2.7	72	GOES, [39]
liquid stratus	radar/radiometer, SFC	0.1	1.9	54	MODIS, [24]
D_e, cirrus	radar, SFC	-5.8	6.5	9	MODIS, [26]
water path		*gm^{-2}*	*%*		
liquid stratus	radar/radiometer, SFC	10.7	32	72	GOES, [39]
liquid stratus	radar/radiometer, SFC	11.3	29	54	MODIS, [24]
cirrus	radar/radiometer, SFC	1.7	22	6	GOES, [25]
cirrus	radar, SFC	0.2	50	9	MODIS, [26]

NA – not available, for these cases VISST – X represents a range in zonal mean differences

at high VZAs. A potentially larger source of bias error is the scattering phase function, which, if not perfectly representative of the crystals within the cloud, will cause biases at certain scattering angles. Since a systematic underestimate of cloud radiating height is due to overestimating the emissivity, the value of τ would have to be overestimated or the factor of ~0.5 used to convert the 0.65-μm optical depth to its 10.8-μm equivalent is too large. An overestimate of τ would imply that the asymmetry factor of the scattering phase function g is too large because, for a given optical depth, the overall reflectance increases with increasing g (e.g., [33]). This impact is discussed further in Section IV.B.2.

At night, the scattering phase function and ozone have minimal impact on the SIST retrievals, which depend only on thermal radiation. The 29 nocturnal retrieved thin-cirrus heights plotted in Fig. 11c are markedly different from those in Fig. 11a. All values of Z_c are greater than Z_{Rb} and one-third of the values exceed Z_{Rt}. Overall, Z_c - Z_{Rb} and Z_c - Z_{Rt} are 2.6 and -0.4 km, respectively. Again, the temperatures (Fig. 11d)

are consistent with the height results. Examination of the time series (not shown) revealed that, when $Z_c > Z_{Rt}$, $\tau < 1$. The SIST is sensitive to errors in the assumed surface temperature and emissivities, and atmospheric corrections in all three channels that can offset or enhance each other. A systematic underestimate of the skin temperature or the 10.8-μm surface emissivity can cause an overestimate of Z_c. Additionally, the cloud radar when used alone often underestimates the ice-cloud top heights because the tops are often composed of undetected small ice crystals. Such an effect would also occur during the day suggesting that the daytime biases could be even larger than noted earlier. Understanding and quantifying these various effects will require a more detailed study than is possible in this paper.

3) All clouds: Comparisons of all single-layer cloud heights from GOES over the SCF showed that, on average for the CPRS applied during day and night, Z_t underestimates the radar-based cloud top height by 0.7 ± 1.4 km [29]. Xi et al. [34] examined long-term averages from GOES for all clouds, single- and multilayered, over the SCF and found that the SIST yields uppermost cloud-top distributions that are in
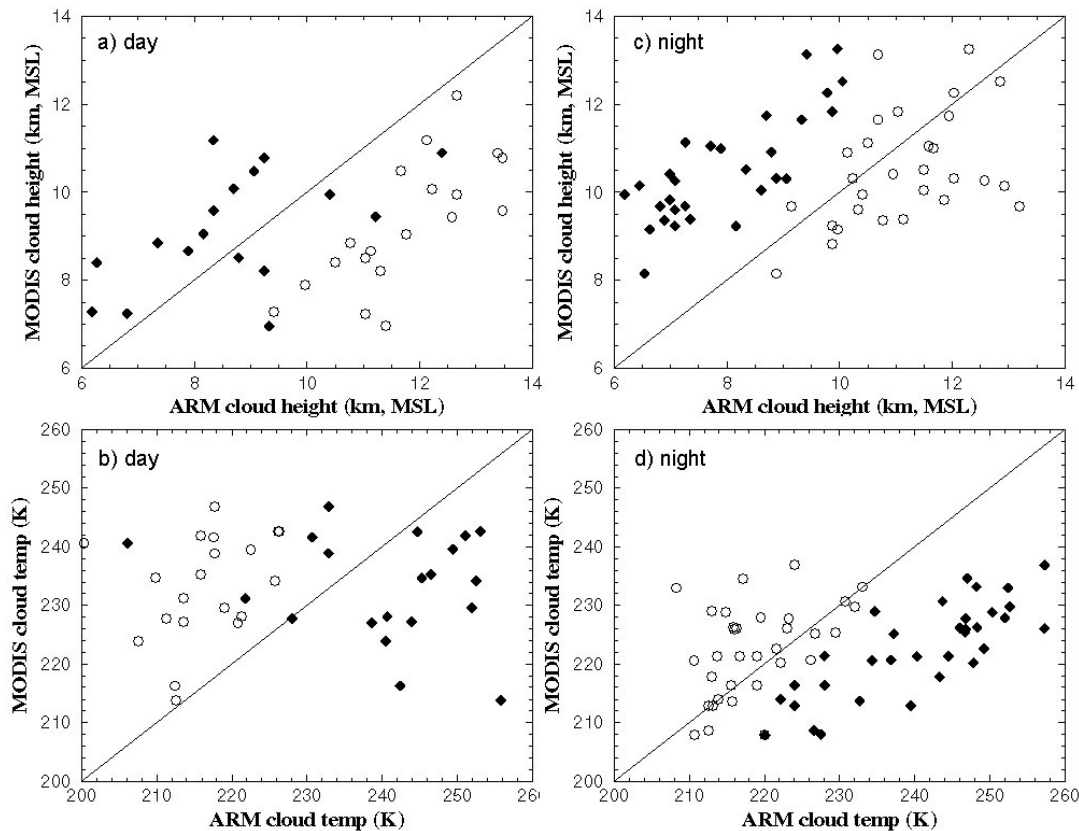
Fig. 11. Overcast single-layer cirrus cloud height and temperature comparisons over ARM SCF for Z_c and T_c from CERES-MODIS retrievals using Aqua and Terra data and cloud boundaries from the ARM Mace PI Product, March 2000 – December 2002. Solid diamonds: ARM cloud base heights and temperatures. Open circles: ARM cloud top heights and temperatures.

relatively good agreement with the radar observations for high clouds. However, the VISST tends to underestimate the occurrence of high cloud tops, finding too many middle and low clouds, primarily as a result of overlapping thin-high-over-thick-low clouds and underestimation of single-layer, ice cloud top heights as reported by [29].

Comparisons of the VIRS and Mace radar-lidar heights for all overcast single-layer clouds over the ARM SCF are shown in Fig. 12 for data taken between January 1998 and June 2001. On average, for optically thick clouds ($\tau > 5$), Z_c is 0.3 ± 1.2 km and 0.2 ± 1.0 km below cloud top during the day (Fig. 12a) and night (Fig. 12c), respectively. In both cases, Z_c is located ~0.5 ± 1.5 km above the mean cloud height, $Z_{Rm} = 0.5 * [Z_{Rt} + Z_{Rb}]$. For optically thin clouds ($\tau < 5$), the inclusion of the low and midlevel reduces the daytime differences (Fig. 12b) between Z_c and Z_{Rt}, relative to those in Fig. 11, to only 1.4 ± 1.6 km. The differences for the high clouds are similar to those in Fig. 11a. For optically thin low clouds, Z_c is generally very close to Z_{Rm}, but is less than Z_{Rm} for clouds above 4 km, meaning it is closer to the cloud bottom than the top as discussed earlier. Similar behavior is seen at night (Fig. 12d) for optically thin low and midlevel clouds, but the high clouds behave more like those in Fig. 11c. Overall, Z_c is only 0.2 ± 1.3 km less than Z_{Rt} and 0.4 ± 1.3 km greater than Z_{Rm}, indicating it is closer to the top than the base. Overall, the VIRS and MODIS results are very consistent compared to the SCF active sensor measurements. Figure 13 shows the autumn 2003 global distributions of average uppermost cloud heights,

Z_t from GLAS and Z_c from CERES-MODIS and their differences for all times of day. Although the GLAS averages (Fig. 13a) are noisy because of the sparse spatial sampling by its nadir-viewing lidar, similarities in the regional mean height distributions are evident. In areas where high clouds are predominant, the lidar cloud tops are mostly higher than their CERES counterparts (Fig. 13b) by more than 8 km in some cases (Fig. 13c). This underestimate by CERES is also apparent in polar regions. In areas where high clouds are sparse, especially in the marine stratus regimes off the subtropical west coasts of the continents, the agreement is much better. Both datasets show the lowest clouds near the coasts with greater heights to the west in most cases. Overall, the average differences (Fig. 13d) are greatest over land in the Tropics rising up to 5 km and up to 4 km over ocean. Around 20°S, the differences are ~1 km, then rise to ~1.4 km over the midlatitudes and up to 2 km over the South Pole. The minimum difference in the Northern Hemisphere is ~1.6 km at 30°N. The bias increases from there up to nearly 4 km at the North Pole. Overall, the mean bias is 2.4 km: 2.3 km over water and 2.7 over land. Comparable, though perhaps smaller, biases were found in a preliminary comparison of CERES-MODIS and CALIPSO data [30].

There are many reasons for the large biases. Accounting for the difference between Z_c and Z_t would diminish the bias by an average of ~ 0.2 km. The underestimate in Z_c for thin cirrus clouds noted earlier will certainly cause some of the underestimation. A potential contributor to the biases in the
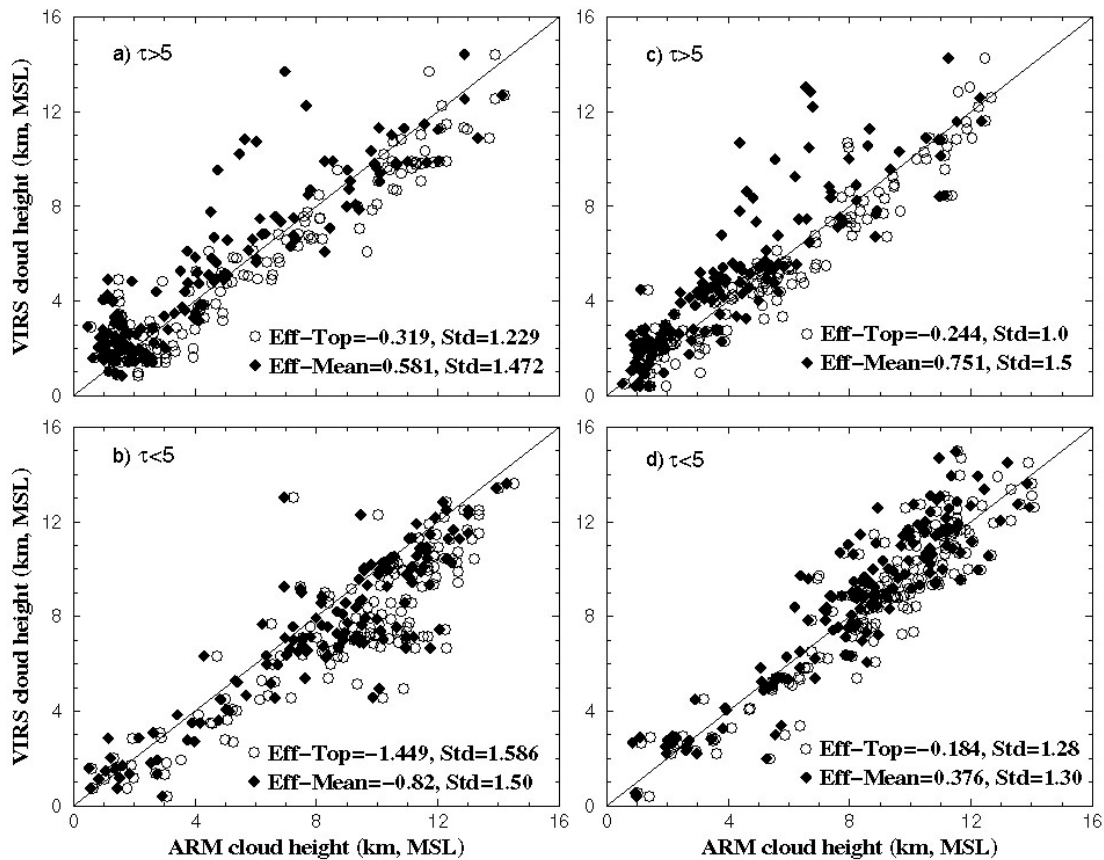
Fig. 12. Overcast single-layer cloud height comparisons over ARM SCF using CERES VIRS Z_c retrievals and ARM ARSCL cloud boundaries during (a, b) daytime and (c, d) nighttime, January 1998 – June 2001.

Tropics, particularly over land, is the orbit of ICESat during October 2003. Most convection over land peaks during the late afternoon and evening resulting in the highest cloud tops during those times [35], [36]. Very deep convection over ocean is most common after midnight, peaking near sunrise [37], [38]. The ICESat orbits are closer to the peak times than either Terra or Aqua and, therefore, should have higher mean cloud top heights than the MODIS retrievals. The magnitude of the difference is unlikely to account for more than 0.5 km or so. All of the comparisons between lidar-radar and the VISST/SIST retrievals have been for overcast, single-layer clouds. If the cloud does not fill the pixel, its height is often underestimated. For low clouds, the lapse rate used to assign height may be too large for some areas. Over the ARM SCF, Dong et al. [24] found that the boundary-layer lapse rate should be closer to -5.5 K km^{-1}, rather than the -7.1 K km^{-1} used in Ed2 for all areas. This effect would be even greater in polar regions where the atmosphere is closer to isothermal than elsewhere. The single lapse rate value is probably a large factor in the polar height biases, at least for optically thick clouds.

Multi-layer cloud systems are also likely to cause underestimates in the retrieved heights when the upper cloud is optically thin. Figure 14 plots the layering statistics for the GLAS observations used in Figure 13. The multilayer cloud occurrence frequencies in Fig. 14a reveal that thin clouds occur over lower clouds up to 60% of the time in some locations. The maxima occur in deep convective areas and the

midlatitude storm tracks. The single-layer mean cloud heights (Fig. 14b) look more like the CERES average heights (Fig. 13b), but are still greater than CERES in the deep convective areas and polar regions. When multi-layer clouds appear, the highest observed cloud (Fig. 13c) is greater than the CERES average height for a given region. Many of those clouds have optical depths < 0.3 and would have minimal impact on the MODIS radiance. The lowest cloud tops in those same cases (Fig. 14d) are generally less than the single-layer mean heights. Thus, in the instances when the uppermost cloud is extremely thin, the MODIS-observed radiance would appear to mostly come from the lower cloud and the retrieval would underestimate the top height by the extreme differences seen in the Tropics.

Table III summarizes the mean cloud heights for the various cases. Overall, the differences between CERES and GLAS are nearly the same for Aqua and Terra, ~2.4 km globally and ~2.1 km in the polar regions. Even compared to the GLAS single-layered clouds, the CERES mean heights are ~0.9 km less. For the multi-layered clouds, the CERES mean heights are nearly 5 km below the highest layers globally and 0.4 km above the lowest layers in the non-polar regions. In polar regions, the CERES and lowest heights are nearly the same. These results show that the multilayered clouds cause some of the most significant differences between the CERES and GLAS cloud heights. However, because the GLAS single-layered clouds are, on average, higher than the CERES mean effective heights, the sources of error (e.g., lapse rate, ice
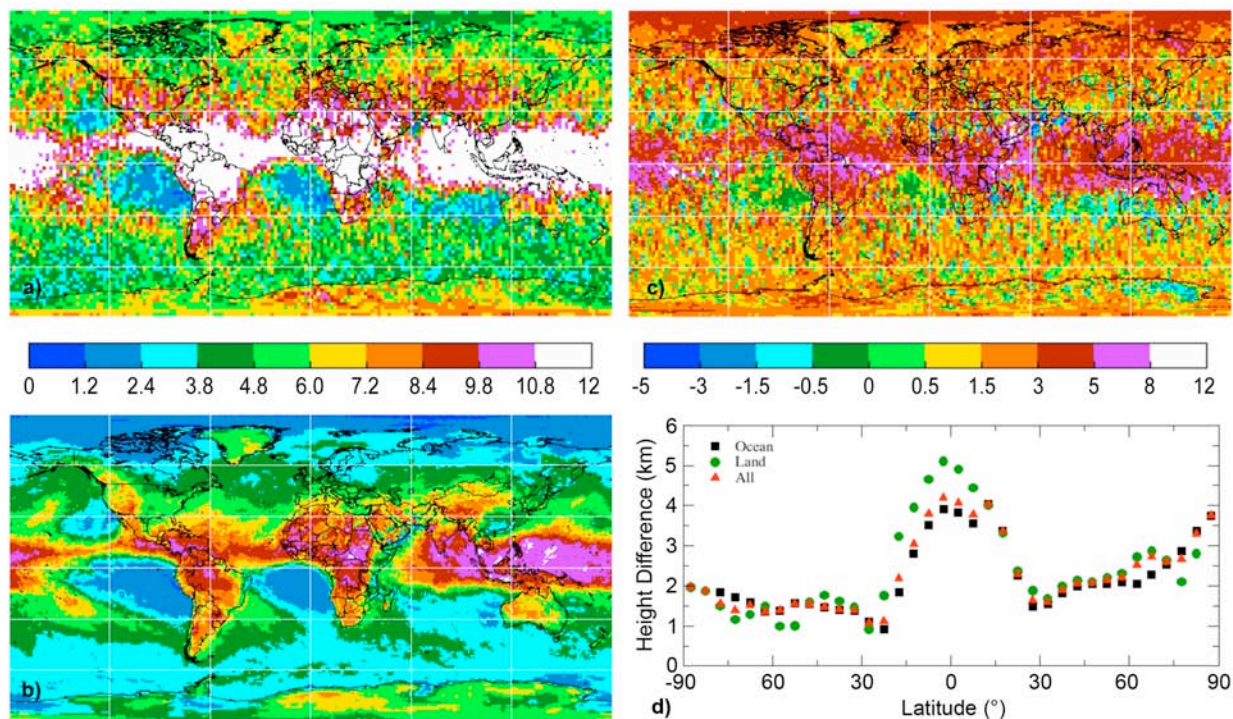
Fig. 13. Comparison of mean (a) ICESAT GLAS uppermost cloud-top heights and (b) CERES-MODIS effective cloud heights and their (c) global and (d) zonal differences, 28 September – 19 November 2003.

cloud optical depth, Z_c vs. Z_t) discussed above likely account for ~1 km in the average difference. Reducing those biases will require addressing all of those sources including the multilayered clouds.

B. Cloud microphysical properties

1) Liquid clouds: The most detailed analyses of liquid cloud properties, to date, have been performed using single-layer, overcast stratus clouds. Comparisons of VISST retrievals from 36-h of GOES-8 and coincident surface-based radar and radiometer data yielded mean differences (GOES – surface) in r_e, τ, and LWP of 1.4 ± 2.7 µm, -2.6 ± 17.6, and 11 ± 84 gm^{-2}, respectively [39]. The corresponding rms differences are 31, 40, and 32%, respectively. Similar comparisons using CERES-MODIS results (CERES – surface) from 2000 – 2004 for stratus clouds over the SCF [24] yielded r_e, τ, and LWP differences of 0.1 ± 1.9 µm, -1.3 ± 9.5, and 0.6 ± 49.9 gm^{-2}, respectively, for Terra and 0.2 ± 1.9 µm, 2.5 ± 7.8, and 28.1 ± 52.7 gm^{-2}, respectively, for Aqua. Overall, the corresponding rms differences are smaller (23, 25, and 30%) compared to the GOES differences from [39], presumably because the spatial and temporal matching and single-layering selections were better for the MODIS comparisons. The larger mean difference for Aqua can be attributed to its 0.64-µm channel gain being 1-2% greater than its Terra counterpart [28]. Several other studies have examined the Ed2 CPRS-retrieved liquid droplet cloud microphysical properties. Comparisons of a few GOES VISST retrievals with those from various types of surface measurements for thin clouds suggest that τ and LWP are underestimated for clouds having LWP < 80 gm^{-2} [40]. Dong et al. [41] compared two SINT retrievals of τ and r_e using data from the second Along-Track Scanning Radiometer

with surface-based radar-radiometer retrievals over Arctic Ocean ice. They found differences similar to the VISST retrievals over the SCF for one case and mixed values for the other due to inhomogeneities in the cloud field.

The microphysical properties retrieved from VIRS using the CPRS for the cases in Fig. 12 were compared with their counterparts retrieved from the passive and active instrumentation at the ARM SCF. The results are summarized in Table IV for daytime and nighttime (shown in parentheses) separately. During the daytime, the values of r_e are weakly, but positively correlated, differing by only -0.2 µm. The optical depths are well correlated ($R^2 = 0.85$) and differ by only 1 (4%). These two parameters translate to somewhat lower correlation for LWP ($R^2 = 0.73$), but the CERES mean is only 8 gm^{-2} (6%) less than the ARM value. These results are comparable to those from matched MODIS and ARM data [24], except that the VIRS averages are slightly less than instead of greater than the ARM data. At night, the correlation between the two measurements essentially disappears because of the SIST optical depth limitations ($\tau < 5$ only). The smallest optical depth from the ARM data is 7.5.

TABLE III.
AVERAGE CLOUD HEIGHTS (KM) FROM GLAS (TOP HEIGHT) AND CERES-MODIS (EFFECTIVE HEIGHT) DATA, 25 SEPTEMBER -18 NOVEMBER 2003.

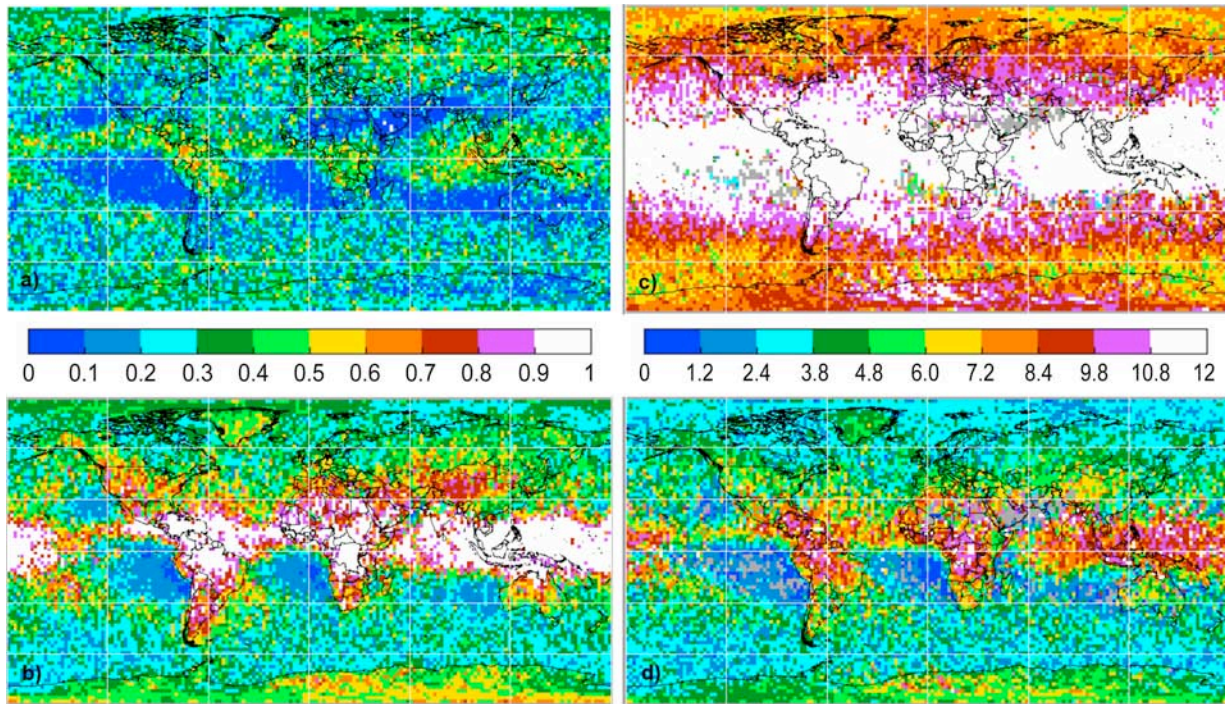| Data	Global	Polar	Non-polar
GLAS highest top, all	7.6	5.4	7.9
CERES Terra, all	5.2	3.3	5.5
CERES Aqua, all	5.3	3.4	5.5
GLAS top, SL	6.4	4.2	6.7
GLAS highest top, ML	11.2	7.9	11.7
GLAS lowest top, ML	4.9	3.5	5.1
Fraction ML	26.6%	30.6%	26.0%

Fig. 14. Average cloud layering statistics from ICESat GLAS for October 2003, (a) fraction of cloudy scenes having multiple layers and mean top heights (in km, see color bar on right) of (b) single-layer clouds and (c) lowest and (d) highest clouds when multiple layers are present.

To further examine the LWP retrieved by the VISST, Fig. 15 plots the CERES SSF and ARM MWR LWPs taken at Pt. Reyes, CA. Only 19 Aqua and 21 Terra footprints met the criteria outlined in Section II.B. The results yield mean differences (CERES – MWR) of 10.0 and 5.6 gm^{-2} for Terra and Aqua, respectively. The corresponding standard deviations of the differences are 38 and 41 gm^{-2}, which translate to 35 and 43% of the respective mean MWR values. The squared correlation coefficients R^2 for Terra and Aqua are 0.54 and 0.55, respectively. For both Terra and Aqua, the average bias (~11%) is comparable to that found for continental stratus over the ARM SCF, but the correlations are lower and the scatter is greater than that from the SCF comparisons [24]. This is not surprising given the coastal

location of the surface site, the large spatial variation of the background albedo and surface temperature, and the comparison with SSF data rather than with carefully matched pixel averages.

The AMSR-E comparisons provide for a broader examination of the VISST LWP retrievals over water surfaces. Figure 16 shows scatterplots of the mean July 2004 LWP values determined for 1° x 1° regions computed from matched Aqua and AMSR-E data for AMSR-E footprints meeting the criteria specified in section II.A.3 using the EOS algorithm for AMSR-E and the VISST for CERES. The statistics computed from the global and northern midlatitude scatterplots are listed in Table V along with those for the other zones, Tropics (20°S – 20°N), southern midlatitudes (60° - 20°N), and high midlatitudes and similar results using the Lin algorithm. Globally, the VISST regional averages compared to those from Fig. 16a have a squared correlation coefficient R^2 of 0.59 with a mean bias of -0.2 gm^{-2} or 0% and a standard deviation σ of 53.6 gm^{-2} or 45%. Over the northern midlatitudes (Fig. 16b), the VISST underestimates the AMSR-E LWP by 32.7
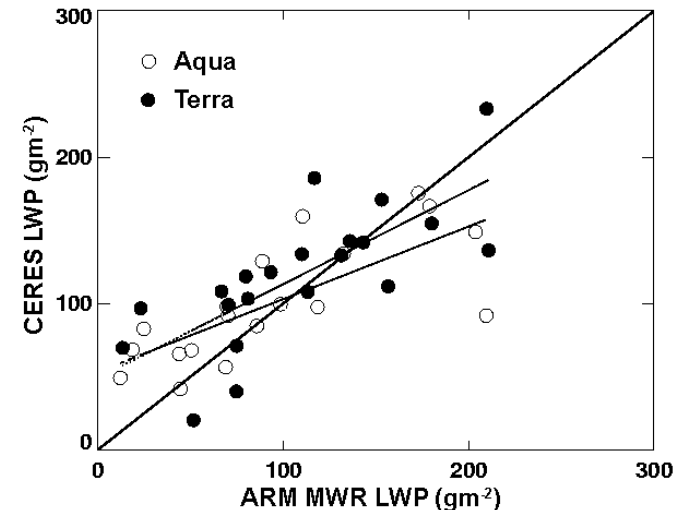

Fig. 15. Comparison of cloud LWP over the ARM Mobile Facility at Pt. Reyes, CA for selected days during March 1 – September 14, 2005 using CERES SSF data.

TABLE IV.
DAYTIME (NIGHTTIME) CLOUD MICROPHYSICAL PROPERTY COMPARISONS FOR OVERCAST STRATUS AND CIRRUS CLOUDS OVER THE SCF FROM CERES-VIRS AND ARM SURFACE INSTRUMENTS, JANUARY 1998 – JUNE 2001.

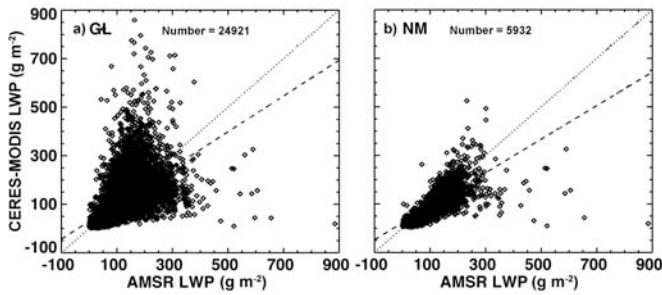| Parameter	Samples	R^2	ARM	CERES
Stratus, r_e (μm)	60 (38)	0.34 (-0.03)	9.0 (8.0)	8.8 (10.2)
Stratus, τ	60 (38)	0.85 (0.1)	24.5 (18.9)	23.5 (8.5)
Stratus, LWP (gm^{-2})	60 (38)	0.73 (0.23)	141 (95.3)	133 (53.6)
Cirrus, D_e (μm)	49 (59)	0.08 (-0.29)	38.2 (36.6)	30.1 (42.5)
Cirrus, τ	49 (59)	0.53 (0.68)	0.9 (0.8)	1.3 (1.1)
Cirrus, IWP (gm^{-2})	49 (59)	0.65 (0.59)	19.3 (18.1)	23.3 (21.1)

Fig. 16. Scatterplots of matched daytime mean 1° x 1° LWP from the EOS algorithm applied to AMSR-E data and the CERES VISST applied to Aqua MODIS data for AMSR-E fields of view containing overcast, non-precipitating liquid water clouds over water during July 2004: (a) global (60°S – 85°N) and (b) northern midlatitudes (20°N – 60°N). Dotted line denotes line of perfect agreement. Dashed: linear fit.

gm^{-2}, but is more correlated with the EOS results than all of the data taken together, $R^2 = 0.79$. The strongest correlation is found for the Tropics, where the greatest biases are found. The differences between the VISST and Lin results are similar, but the VISST underestimate is larger. Limiting the data to only those fields of view having $T_c > 273.15$ K (Table V, right side) increases the correlation everywhere except over the Tropics. However, the biases tend to increase while the standard deviations of the differences remain steady or decrease. The bias is positive for the northern high latitudes and southern midlatitudes and negative everywhere else.

Figure 17 shows the matched mean zonal CERES and AMSR-E LWPs for July 2004 (Fig. 17a) and their differences (Fig. 17b) and the differences for the subset consisting of all cases having $T_c > 273.15$ K (Fig. 17c). The differences are not the same as the global values in Table V because the actual area of the 1° regions was accounted for in the averaging process. Figure 17d plots the August 2007 mean zonal differences between CERES-MODIS Ed2 and Edition 3-beta2,

which corrects the ozone absorption errors in Ed2, for all liquid water clouds. Although both AMSR-E averages are relatively constant outside of the tropics, the VISST values tend to increase north of 60°N and south of 35°S (Fig. 17a). Furthermore, the AMSR-E LWPs have more dramatic peaks between the Equator and 10°N than their CERES counterparts. On average, the Lin AMSR-E values are ~12 gm^{-2} greater than their EOS counterparts and differ by as much as 30 gm^{-2} in some zones (Fig. 17b). While the mean difference between the VISST and EOS LWPs is only 3 gm^{-2}, the zonal differences range from -55 gm^{-2} at 7.5°N to 145 gm^{-2} at 60°S. These extremes are beyond the greatest zonal differences between the two AMSR-E retrieval methods. When supercooled clouds are removed (Fig. 17c), the biases increase in magnitude, mostly in the southern midlatitudes.

The negative biases in most areas are surprising given the mostly positive biases found to date using the surface-based MWR data. However, a 2% underestimate of LWP from the VIRS VISST relative to the TRMM Microwave Imager was found over the oceans between 38°S and 38°N [42]. Perhaps, some of the discrepancy is due to differences in the retrievals from up- and downlooking MWRs. The large tropical CERES-AMSR-E differences could arise for several reasons. In the Tropics, the mean values of τ and/or r_e from CERES could be too low or the LWP from AMSR-E could be too large. A sensitivity study [43] of the AMSR-E retrievals reveals that, for areas with total precipitable water (PW) exceeding 6 cm, the LWP can be overestimated by 50 gm^{-2} or more. The maximum difference for the Tropics in Fig. 17b occurs where PW > 6 cm. Thus, systematic errors in the microwave retrievals could account for, at least, some of the large discrepancies in the Tropics. When computing LWP, the

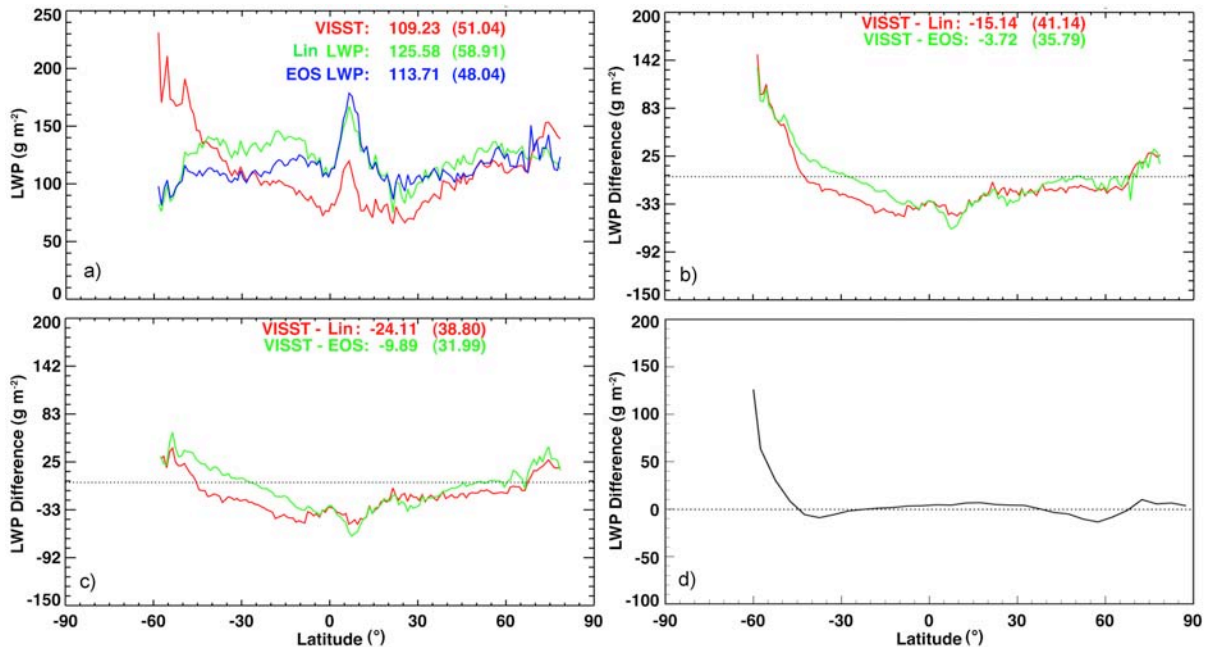Fig. 17. Monthly mean zonal (a) July 2004 liquid water path and differences between (b) CERES-MODIS and AMSR-E retrievals for all overcast, non-precipitating liquid water clouds over ocean observed from Aqua MODIS when the sunglint probability is < 5%, and (c) for the subset of cases having $T_c > 273.15$ K, and between (d) August 2007 Ed2 and Edition 3-beta 2 CERES-MODIS retrievals from Terra for all ocean liquid clouds.

TABLE V.
REGURAL (1° X 1°) DIFFERENCES BETWEEN AQUA AMSR-E LWP AND DAYTIME CERES LWP (CERES – AMSR-E) FOR OVERCAST LIQUID WATER CLOUDS OVER WATER, JULY 2004.

Domain	All Clouds			T_c > 273.15 K		
Lin	R^2	Bias, gm⁻² (%)	σ, gm⁻² (%)	R^2	Bias, gm⁻² (%)	σ, gm⁻² (%)
Global (60°S – 85°N)	0.60	-11.7 (9)	56.6 (45)	0.76	-23.4 (-19)	42.8 (34)
20°S – 60°S	0.53	8.8 (7)	62.1 (49)	0.78	-14.4 (-11)	38.8 (30)
20°S – 20°N	0.79	-40.0 (-30)	46.7 (36)	0.80	-40.9 (-31)	47.0 (36)
20°N - 60°N	0.80	-16.8 (-15)	36.7 (32)	0.80	-16.0 (-14.8)	37.0 (33)
60°N – 85°N	0.69	6.8 (5)	32.1 (26)	0.78	9.0 (8)	28.6 (27)
EOS						
Global	0.59	-0.2 (0)	53.6 (48)	0.71	-8.3 (8)	40.9 (37)
20°S – 60°S	0.66	27.9 (26)	54.6 (51)	0.80	12.3 (12)	35.9 (35)
20°S – 20°N	0.80	-32.7 (-26)	39.6 (32)	0.79	-32.9 (-27)	40.6 (33)
20°N - 60°N	0.74	-12.7 (-11)	35.9 (32)	0.79	-10.9 (-10)	29.9 (28)
60°N – 85°N	0.08	3.7 (3)	83.5 (66)	0.33	17.3 (18)	60.1 (62)

CPRS assumes that r_e based on the 3.8-μm radiance is uniform throughout the cloud. Since the 3.8-μm retrieval represents the value at the top portion of the cloud, the actual vertical profile of droplet radius within the cloud will determine whether the LWP estimate is too high or too low. Near-infrared channels can be used to estimate the droplet size profile [44], [45] and retrieve a better estimate of LWP and information about drizzle [46]. In cases where the 3.8-μm r_e is smaller than the NIR values, the clouds are typically drizzling [47] and the CPRS LWP may be too low. The differences between the MAST 1.6 and 3.8-μm retrievals are greatest in Tropics particularly in the Intertropical Convergence Zone, where the CPRS underestimate is the largest [48]. This suggests that the bias is, at least, in part due to the use of 3.8-μm observations to estimate r_e. If the clouds in Tropics are mostly precipitating, then the AMSR-E LWP also becomes more uncertain because the microwave retrieval algorithm is sensitive to the presence of rain [48].

In the southern midlatitudes, the positive differences could result from overestimates of τ and/or r_e by CERES due to large SZAs or underestimates by AMSR-E due to high wind speeds and low PW values [43]. As noted in section III.A, the ozone optical depth underestimation in the VISST retrievals causes an overestimation of τ. This overestimate is enhanced at large SZAs because the change in reflectance with τ increases with rising SZA [33] and the error in the ozone path length [9] increases with SZA. Figure 17d provides an estimate of the effect of that error. It shows the differences between the CERES Ed2 and Edition 3-Beta2 Terra LWPs for all liquid clouds observed over ocean for August 2007 (only 1 month of Edition 3-Beta2 data is available and only for Terra). Inclusion of the proper ozone absorption correction alters the LWP field by only ±10 gm⁻², except at the southernmost latitudes where the SZAs are largest. The overall change in LWP from Ed2 to Edition 3-Beta2 is only 2.5 gm⁻², but exceeds 100 gm⁻² at 60°S where the largest differences are seen in Fig. 17b. Thus, it is clear that much of the increase with latitude in the southern hemisphere is due to the

atmospheric correction error. Similar changes are expected in the higher latitudes of the northern hemisphere during boreal winter and in the highest latitudes of both hemispheres during the equinoctial seasons. Thus, the CERES-MODIS LWP and IWP retrievals are biased at high latitudes, when the VISST is used at large SZAs. The LWPs retrieved over snow and ice surfaces using the SINT have not yet been evaluated, but differ by a factor of two between Aqua and Terra as noted earlier.

2) Ice clouds: Both in situ and active remote sensing measurements have been used to evaluate the VISST and SIST retrievals. GOES VISST and radar-radiometer retrievals of cirrus microphysical properties at the SCF yielded mean differences of 13% and 3% in τ and IWP, respectively, for 6 cases having means of 1.7 and 56 gm⁻² [25]. Similar comparisons using CERES-MODIS retrievals from 9 Terra overpasses found that the VISST produced biases of 15%, -18%, and -16% in τ, D_e, and IWP, respectively, for τ < 2 [26]. A larger overestimate of ~29% in the GOES VISST τ relative to that determined from a narrowband radiometer was found for 47 cirrus cloud samples over the SCF [49]. Except for one case of mismatched data, τ and IWP from GOES were well within the ranges of a variety of retrievals using different surface instruments at the SCF [50].

Table IV summarizes the cirrus cloud properties derived over the SCF from the VIRS and ARM data used in Fig. 12. During daytime, the particle sizes are poorly correlated and underestimated by CERES relative to the surface retrieval by 8 μm (21%). The optical depths have a greater correlation, but it is less than that found for the daytime stratus clouds. Moreover, the CERES average τ is 0.4 or 44% greater than that from the surface. Surprisingly, the IWPs are more correlated than the other two parameters. Overall, CERES yields IWP values that are 4 gm⁻² (21%) greater than their ARM counterparts. These results are more like the GOES-ARM comparison by Min et al. [49]. At night, the overestimate in τ relative to the ARM retrieval is smaller than during the day, contrary to what would be expected based on
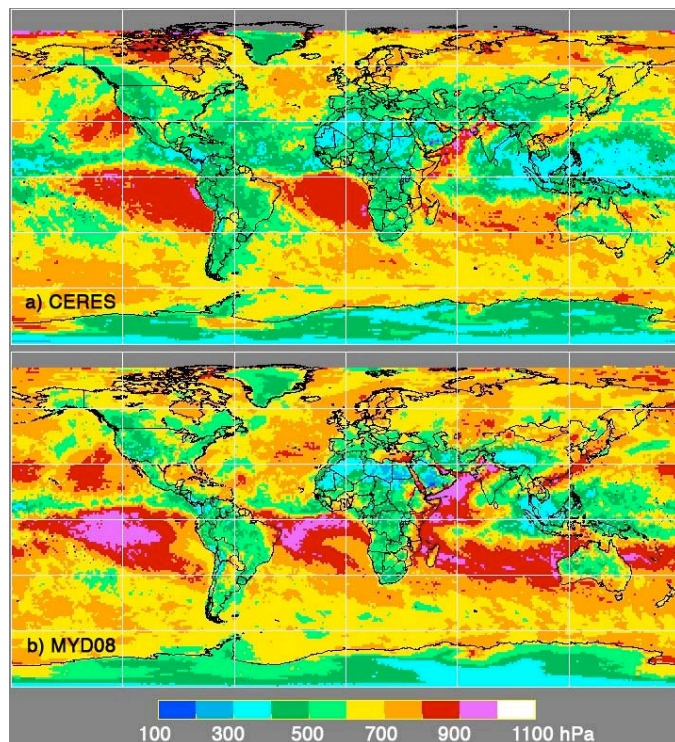
Fig. 18. Mean daytime cloud-top pressure p_t from Aqua MODIS data, October 2003.

the differences in cloud-top heights seen in Fig. 12d.

The overestimates in the VISST cirrus optical depths range from 13 – 44% causing a daytime bias in Z_c, as discussed in Section IV.A.2. The biases are larger for VIRS and GOES. Part of the greater τ biases in Tables II and IV and [49] is due to underestimates in the Rayleigh scattering and overestimates in the ozone absorption parameterizations used in the VISST for the GOES and VIRS visible channels. Both factors tend to cause an overestimate of τ. The Rayleigh scattering error is not a factor for the MODIS retrievals. Additionally, the SZAs for the MODIS observations are generally greater than those for the other two instruments because GOES and VIRS observations cover all times of day rather than the 4 hours around local noon. These angle differences would cause a greater bias due to ozone absorption for VIRS and GOES. Other sources of error in the τ and Z_c retrievals are the parameterizations used in the retrieval, the scattering phase functions as noted earlier, uncertainties in the surface reflectance and atmospheric corrections, and, possibly, the relationship between the infrared and visible optical depths. The reflectance parameterization is unbiased for plane-parallel clouds [9] and it is unlikely that the surface reflectance and atmospheric corrections, other than ozone and Rayleigh scattering, are biased because they are based on direct measurements. Thus, realizing smaller cirrus optical depths would require a smaller asymmetry factor. For medium and large crystals, an optical model incorporating crystals with a roughened surface [51] or embedded air bubbles [52] could yield smaller optical depths at many, but not all, scattering angles. The overall mean τ should drop if such models were used in place of the CERES Ed2 smooth crystal models. If

smaller values of g do not sufficiently reduce τ to achieve accurate values of Z_c, then it may be necessary to examine the relationship between the infrared and visible optical depths.

The overestimates of τ for optically thin clouds are compensated by underestimation of D_e, which results in IWP biases ranging from -16 to 21%. While there have been no one-on-one comparisons of CERES and active sensor IWP for thick clouds, the non-polar regional means from CERES are in reasonable agreement with those determined from CloudSat values that rely on radar data only [27]. Thus, despite the apparent biases seen in the optical depths, CERES seems to yield very reasonable values of IWP. However, it is important to remember that many of the thicker ice cloud cases consist of an ice -over-water cloud system. The total water path in these cases, which consists of both LWP and IWP, is probably underestimated [54] and is not likely to be a good estimate of IWP. Certainly further study is required to fully assess all of the uncertainties in Ed2 ice cloud properties and to reduce them in future editions, especially over polar regions where few studies have been performed.

V. COMPARISONS WITH MAST COLLECTION 5 RETRIEVALS

In this section, mean cloud properties retrieved from 2003 MODIS data are compared to their CERES-MODIS counterparts. A comprehensive comparison of CERES-MODIS cloud retrievals with the MAST results and with other satellite-based cloud retrievals is beyond the scope of this paper. Such an effort is underway as part the Global Energy and Water Cycle Experiment (C. Stubenrauch, personal communication, 2010) and includes satellite-derived cloud properties from a number of other algorithms (e.g., [55] - [58]). The MAST comparisons are presented here because they were generated with the same MODIS data using different algorithms. Both datasets are available to the scientific community, so it is important make users aware of some of the similarities and differences in the two datasets. The example MAST and CERES comparisons shown here are quite typical for other months and years. The subscripts M and C are used to indicate that the parameter refers to the MAST or CERES values. Except for cloud top pressure, the cloud properties are compared only for daytime since the MAST optical property retrievals were only performed during the day. Additionally, it should be noted that each MAST cloudy pixel is associated with a cloud-top pressure, but not always with cloud optical properties.

Figure 18 shows the distribution of mean daytime CERES and MYD08 cloud-top pressures, from Aqua MODIS (Collection 5) data for October 2003. In general, the patterns are quite similar with some notable differences. Over the deep convective areas of the Tropics, p_{tM} is generally greater than p_{tC}. West of South America and southern Africa in the marine stratus regions, the reverse is true: p_{tM} (Z_{tM}, not shown) increases (decreases) from east to west while p_{tC} and Z_{tC} (not shown) follows the opposite trend. In the midlatitudes, differences between p_{tM} and p_{tC} are variable. This is more apparent in the mean difference map for all of 2003 shown in
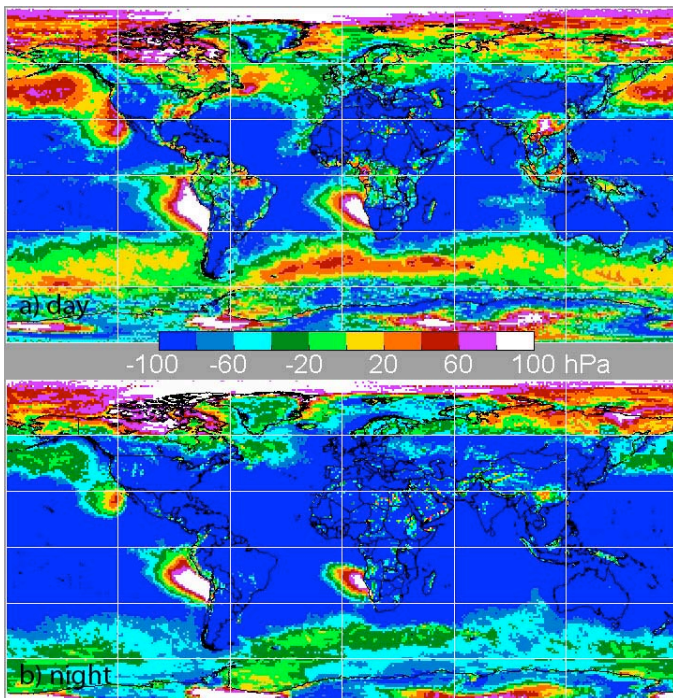
Fig. 19. Differences (CERES Ed2 – MOD08) between 2003 daytime mean cloud-top pressures from Terra MODIS data: (a) day, (b) night.

Fig. 19. The cooler colors indicate that the CERES cloud tops are higher and the warmer colors denote that they are lower than the MODIS retrievals. Over the Arctic, the $p_{tC} > p_{tM}$ by up to 100 hPa, but over all polar regions together is p_{tC} is 27 hPa less than p_{tM}. In the Arctic, the CERES cloud heights were low compared to the GLAS data (Fig. 13d), so the MODIS values are probably less biased there than CERES. Over the northern midlatitudes, p_{tC} is roughly 50 hPa less than its MYD08 counterpart although in some areas over water, it exceeds p_{tM} by as much as 60 hPa. In those same areas, during October 2003 (Fig. 18), p_{tC} is greater than p_{tM} only off the California coast, where Z_{tC} is within a few hundred meters of the GLAS average (Fig. 13c). Over other areas p_{tC} (Z_{tC}) is less (greater) than p_{tM} (Z_{tM}). Over much of the Tropics, p_{tC} is less than p_{tM} by more than 80 hPa. The positive differences are mainly over marine stratus regions as seen in Fig. 18. In the southern midlatitudes, the differences are mainly ± 20 hPa. Farther south, the CERES pressures are less, overall, than the MODIS values in contrast to the Arctic results. Table VI summarizes the differences between the two data products for 2003. The Aqua cloud-top pressures differ more than the Terra values. Presumably, the differences are larger at night because the CERES cirrus heights increase due to an algorithm change and the MAST algorithm remains the same.

The results seem surprising given the findings of [26], but they are more in line with those reported by [29]. Part of the difference may be the inclusion of many trade cumulus clouds in the MAST averages, which were not included in the MAST microphysical retrievals and were missed by the CERES cloud mask [5]. However, even in many of the areas dominated by deep convection and cirrus decks, the differences are mostly less than -80 hPa. The MAST cloud-top pressure is actually an effective pressure because it is based on using an infrared

brightness temperature that corresponds to some depth in the cloud as discussed earlier. Assuming that it is equivalent to the CERES p_c would account for about 40% of the average difference. A more detailed analysis of these differences is beyond the scope of this paper. However, the uncertainties in the MAST cloud top pressure retrievals are discussed at length by [14] and [59].

Mean daytime liquid water cloud optical depths can be compared using Fig. 20. In general, the distributions are very similar, but τ_C is less than τ_M. Some notable exceptions are seen for the Terra results (Fig. 20a, c) in the North Atlantic and over northern Russia. The greatest differences are found over Greenland and Antarctica and its ice shelf. Values of $\tau_C <$ 4 are found over many parts of the tropical oceans while few are seen in the MODIS results for both Terra (Fig. 20c) and Aqua (Fig. 20d). For all of 2003, τ_C is ~2.1 less than τ_M liquid water clouds in non-polar regions (Table VI). This difference jumps up to ~11 and 27 in the polar regions for Terra and Aqua, respectively. The disparity for the two satellites is the result of the errors in the SINT for Aqua noted earlier.

Figure 21 shows the distributions of mean October 2003 ice cloud optical depths. Again, the patterns are very similar with τ_C typically being equal to or slightly less than τ_M. The minimum values of $\tau_C < 1$ occur over large areas in the southern Tropics (Fig. 21a, b). No ice clouds (gray color) are retrieved for either MOD08 (Fig. 21c) or MYD08 (Fig. 21d) over much of those same areas. Few areas have $\tau_M < 1$. Similar to the results in Fig. 20, the largest differences are found over the permanent snow surfaces. On average for 2003, τ_C is ~2.9 and ~13 less than τ_M for ice clouds in non-polar and polar regions, respectively (Table IV).

The differences between the CERES and MODIS optical depths could be the result of a number factors, including the use of different retrieval models and parameterizations, different atmospheric profiles and surface reflectances, and processing decisions. The CPRS uses emittance and reflectance lookup tables based on distributions of solid hexagonal ice columns [33] and retrieves τ using the 0.64-μm channel over land and ocean. The MAST algorithms employ models based on various combinations of ice crystal shapes and sizes [60] and retrieve τ with the 0.86 and 0.64-μm channels over ocean and land, respectively [61]. Over snow and ice surfaces, CERES uses either the 1.6 or 2.1–μm band for τ while MAST uses the 1.24-μm channel. The MAST algorithms rely on the National Center for Environmental Prediction global analyses for temperature and humidity profiles, while CERES uses the Global Modeling Assimilation Office Global Earth Observing System (GEOS) Model 4.03 analyses. These differences will undoubtedly result in different values for τ. Additionally, the maximum values of τ in the CERES and MAST retrievals are 128 and 150, respectively.

A potentially larger source of the biases in non-polar regions, at least, is the number of no retrievals. As noted in [5], the CERES algorithm detects fewer clouds than the MAST mask, but retrieves cloud properties for a greater

Table VI.
Summary of differences (CERES – MAST) in Terra and Aqua daytime mean 2003 cloud properties from monthly average products, MOD08 and MYD08.

Parameter	Terra			Aqua		
	Global	Non-polar	Polar	Global	Non-polar	Polar
T_c (K)	-3.6	-0.8	-3.4	-3.9	-4.0	-3.3
p_t (hPa)	-61.3	-69.0	-11.4	-77.4	-85.2	-26.6
p_t (hPa)*	-122.4	-138.9	-15.5	-129.0	-146.3	-16.6
τ, liquid	-2.9	-1.5	-11.4	-4.1	-2.7	-13.4
τ, ice	-4.0	-2.7	-12.8	-4.6	-3.1	-14.3
r_e (μm)	-2.5	-2.9	-0.1	-2.0	-2.4	0.1
D_e (μm)	1.6	1.0	5.5	0.2	-0.1	2.0
LWP (gm^{-2})	-31.7	-24.4	-79.0	-44.3	-34.9	-104.8
IWP (gm^{-2})	-3.3	18.2	-142.1	-26.3	-2.9	-177.3

* nighttime

number of pixels than the MAST algorithms. This relatively large number of no retrievals is due, in part, to the excision of cloud edge pixels from the cloud retrievals and the possible infrequent retrieval of properties for ice clouds having $\tau < 1$ (e.g., [63]). In the former instance, low-optical-depth edge pixels of large clouds and clouds consisting of only a few pixels would be eliminated, reducing the mean optical depth. The paucity of small optical depth ice clouds would explain the complete absence of ice clouds in some tropical areas as seen in Fig. 21c,d.

An example of this effect is seen in Fig. 22 for a Terra MODIS granule taken over the southeastern Indian Ocean at 0615 UTC, 3 July 2005. The scene (Fig. 22a) includes a section of closed cell stratocumulus on the left side, northeast of an overlying cirrus deck. The eastern half of the scene is dominated by open-celled stratocumulus clouds. The clouds identified as being liquid phase by the CPRS are represented by the droplet effective radius image (Fig. 22b). The MAST cloud mask denoted by the p_{cM} image (Fig. 22c) detected

slightly more cloudy pixels than CERES (Fig. 22d) and placed the open-celled clouds at a greater (lower) pressure (height) than CERES, while some of the close-celled clouds are at lower pressures. Figures 22e and f show the retrieved optical depths from both MODIS and CERES, respectively, for both ice and water clouds. It is clear that quite few open-celled clouds retrieved by CERES are missing from the MODIS product. Many of those clouds have $\tau_C < 1$ or 2. In areas, where distinct holes are evident in the otherwise solid cloud decks, the holes are noticeably larger in Fig. 22e than in Fig. 22f. Again, these generally correspond to small values of τ_C. Another example of the impact of removing edge pixels is shown in [5]. To examine this effect more closely, the differences between τ_C and τ_M for all of the matched pixel data, MOD06 and CERES, from Terra MODIS were computed for non-polar areas for 3 July 2005. The averages differences (τ_C - τ_M) for liquid water clouds are -0.4 ± 3.2 and
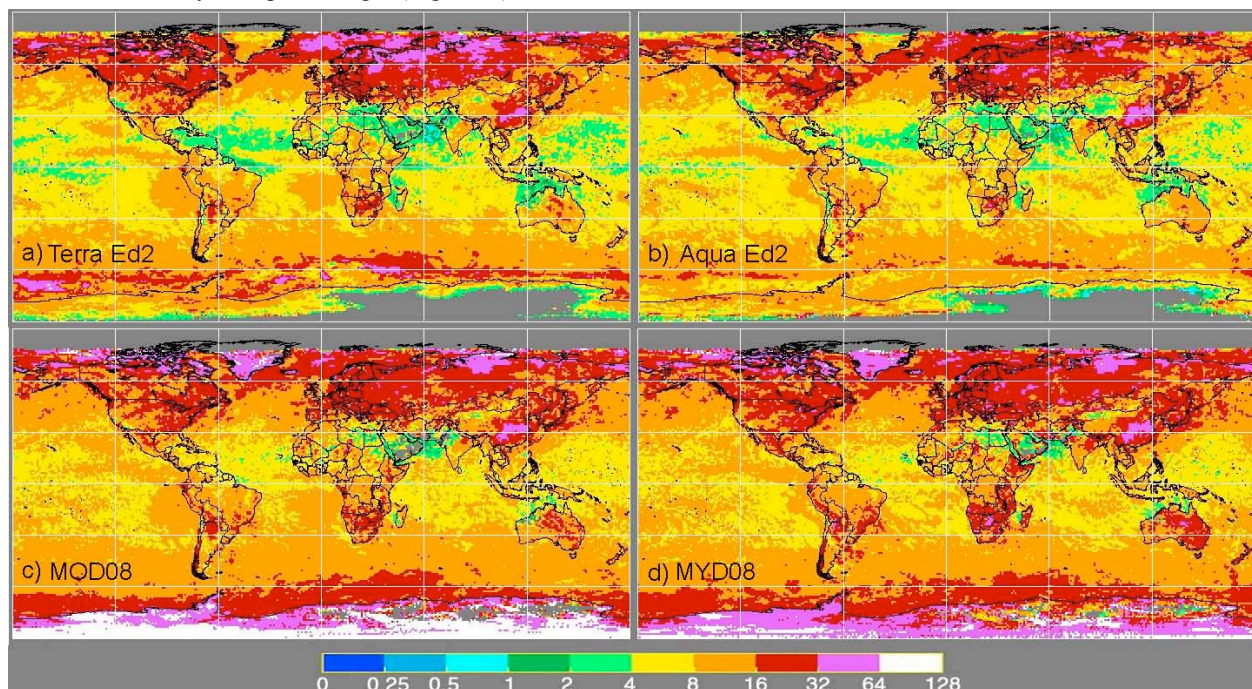

Fig. 20. Mean daytime liquid water cloud optical depth from MODIS data, October 2003.
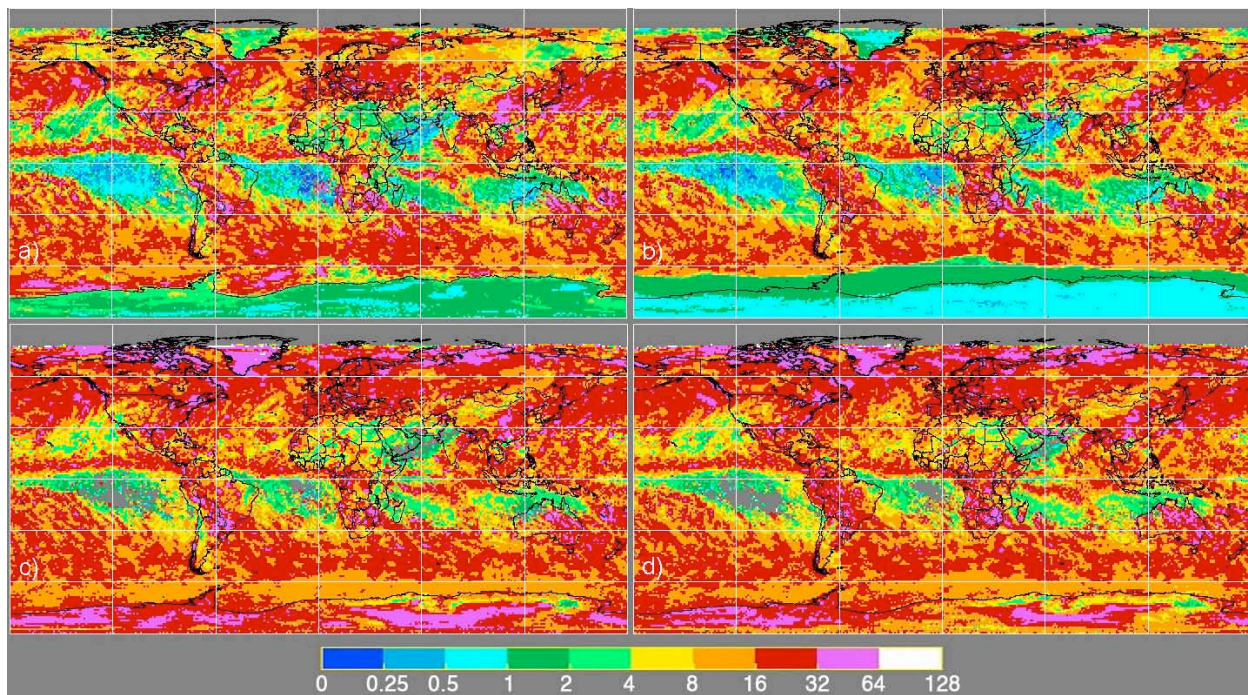
Fig. 21. Mean daytime ice cloud optical depth from MODIS data, October 2003. (a) CERES Terra Ed2, (b) CERES Aqua Ed2, (c) MOD08, and (d) MYD08.

-0.1 ± 3.2 over land and water, respectively. The corresponding differences for ice clouds are -0.1 ± 8.6 and 0.4 ± 9.1. The large standard deviations are most likely the result of the different models and retrieval methods. However, the small biases indicate that the primary cause of the biases in Table VI is the absence of the no-retrieval pixels in the MOD08/MYD08 averages.

The same pixel-level comparison was performed to determine the impact of the unretrieved pixels on the cloud-top pressures. For nonpolar regions, the sign of the p_C - p_M differences is reversed. For ice clouds, the pressure differences are 14 ± 79 hPa and 11 ± 81 hPa over water and land, respectively. The corresponding differences for liquid water clouds are 35 ± 109 hPa and 78 ± 108 hPa. Differences were not computed for clouds that were identified as ice by one algorithm and water by the other. Overall, mismatched-phase pixels account for about 5% of the mutually cloudy pixels. To account for the discrepancy between the results in Table VI and the matched pixels, the unretrieved pixels must be for clouds that are systematically lower than the average of the other pixels. The values of p_M for the unretrieved MOD06 pixels in Fig. 22 are generally greater than 900 hPa, which easily exceeds many of the nearby or coincident values of p_C. These exceedingly high values of p_M for unretrieved low clouds is common in many of the images. It was concluded that many of the unretrieved pixels have relatively small optical depths. Therefore, they are semitransparent and their temperatures require adjustment for emissivity. In the MAST algorithm [14], the top pressure for clouds that have $p_M > 700$ hPa with the CO_2-slicing technique [59], are found by assigning the height corresponding to 10.8-μm brightness temperatures with the assumption of opacity. Thus, many of the unretrieved clouds would have overestimated cloud-top pressures because the brightness temperature is not corrected

for semi-transparency. These extremely low cloudy pixels are included in the monthly average MAST cloud-top pressure product, but are not in the matched pixel-level comparisons. Thus, it is concluded that when both the CERES and MAST algorithms classify a pixel as an ice cloud, the cloud-top pressures are, on average, very close differing by only 12 hPa. However, for phase-matched liquid water cloud pixels, p_C exceeds p_M by ~45 hPa in the mean, which would place the CERES water clouds ~0.45 km below their MSAT counterparts.

The October 2003 mean cloud effective particle sizes are plotted in Figs. 23 and 24. The patterns of r_e are very similar, except that $r_{eM} > r_{eC}$ in most areas. Exceptions include the values over ice-covered surfaces such as the Antarctic ice shelf, Siberia, and the Arctic Ocean. The largest differences are evident over the ITCZ and other tropical marine areas where r_{eM} exceeds 22 μm. The differences over the marine stratus regimes are generally less than 1 μm. The mean 2003 difference (r_{eC} - r_{eM}) is -2.7 μm over non-polar regions and~0.0 over polar areas (Table VI). The CERES and MODIS averages are based on retrievals using the 3.8 and 2.1-μm channels, respectively. Similar results were found by [48] for the differences between the values of r_e retrieved with the MAST algorithms using 3.8 and 1.6 μm radiances; very few negative r_e(1.6 μm) − r_e(3.8 μm) values were observed. The effective radius based on the 1.6-μm retrieval corresponds to a level even deeper in the cloud than that for 2.1 μm. Differences between the values of r_e retrieved with the 3.8-μm radiances using both CERES and MAST algorithms for the 3 July 2005 nonpolar Terra granules yield a mean value of -0.2± 1.9 μm for pixels classified as water by both algorithms. The differences using r_e(2.1 μm) produce an average of -1.2 ± 5.2 μm which is less than half the value in Table VI. This result suggests that many of the missing pixels have relatively small
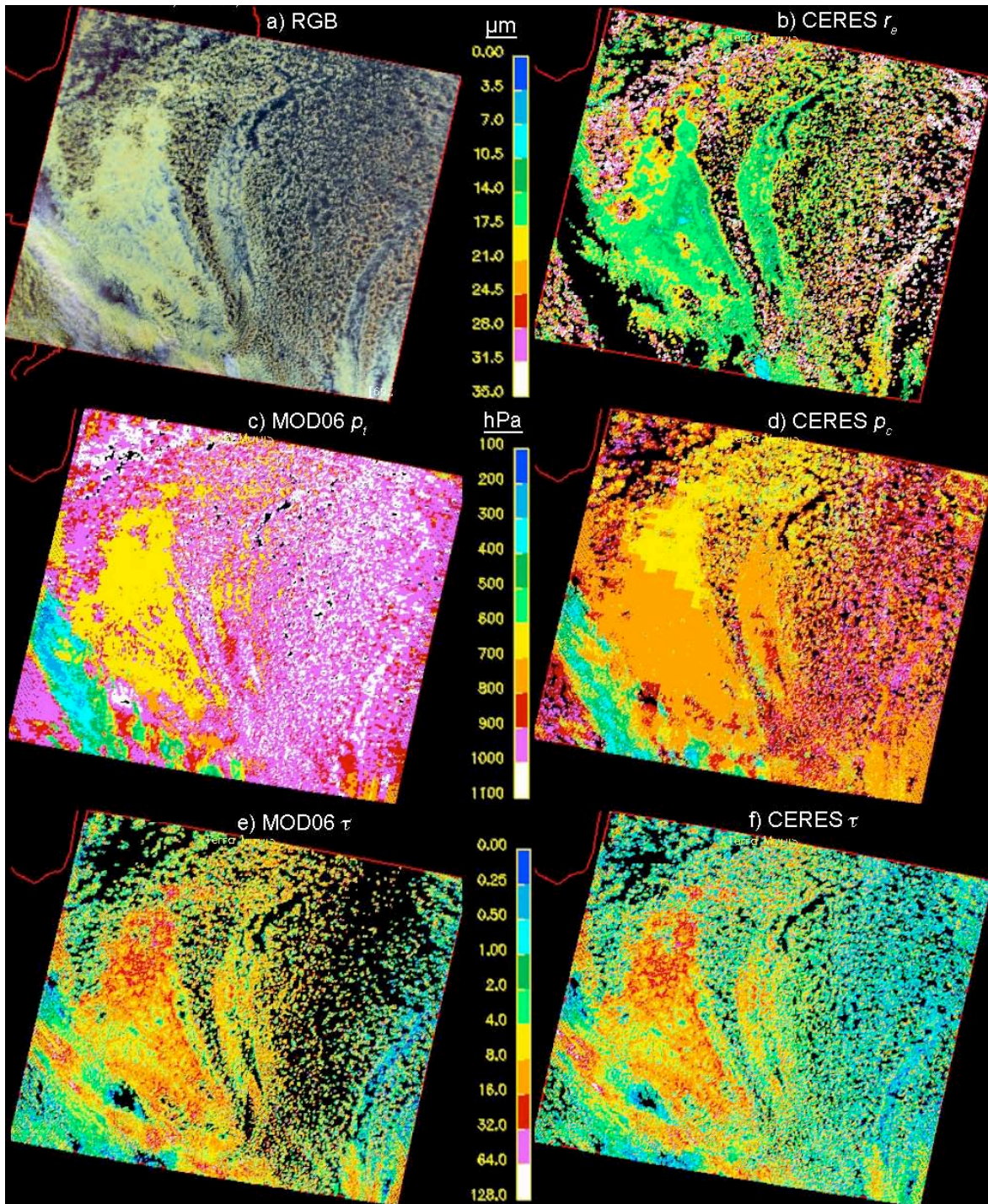
Fig. 22. Pixel-level cloud retrievals from Terra MODIS data over marine stratus clouds centered at 32.4°S, 57.6°E, 0615 UTC, 3 July 2005.

values of r_{eC} and the MAST pixels, which were classified as liquid water but identified as ice clouds by CPRS, had relatively large values compared to the phase-matched pixels. In either the phase matched pixels or the monthly averages, $r_e(2.1 \, \mu m) > r_{eC}$. Thus, it can be concluded that the non-polar r_e differences seen in Fig. 23 and Table VI are due to the use of the two different spectral channels by the two algorithms and to the absence of no-retrievals or mismatches in cloud phase.

The results seen here and in [48] are surprising. Because the 2.1 and 1.6-µm r_e retrievals correspond to locations deeper in the cloud than the 3.8-µm retrieval, the results suggest that, nearly everywhere, smaller droplets are located at the cloud top in opposition to the typical adiabatic profile of non-precipitating clouds. Several recent studies have developed an explanation for this finding based on matched MODIS and CloudSat data [66], [67]. However, determining whether this effect is real and the explanation is correct will require some in situ profiles of droplet distributions in many different clouds coincident with the satellite retrievals.

To compare the ice crystal effective diameters, the MAST values of r_e for ice clouds were simply multiplied by 2. This
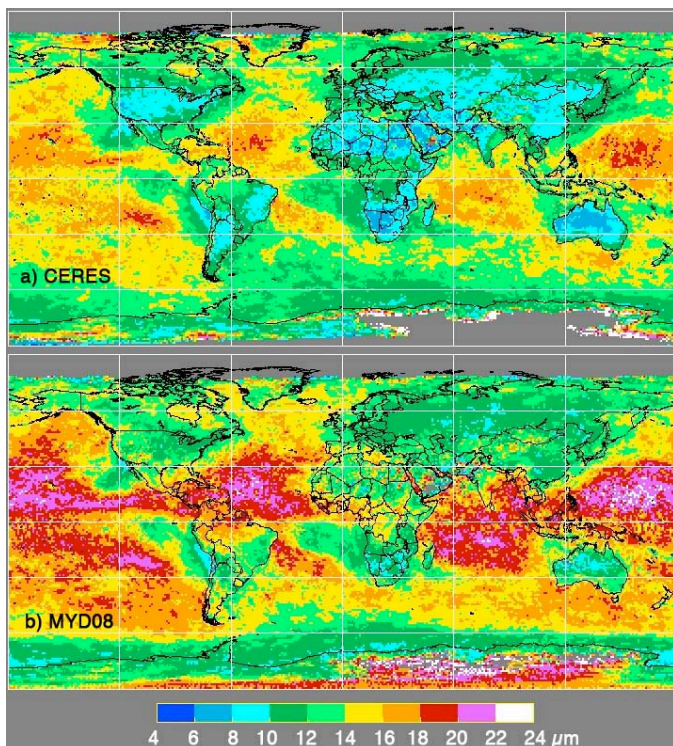
Fig. 23. Mean daytime liquid water effective radius from Aqua MODIS data, October 2003.

Fig. 24. Mean daytime ice crystal effective diameter from Aqua MODIS data, October 2003.

approach yields values of D_{eM} that are within ~ 1 µm of D_{eC} for D_{eC} = 50 µm. The results are shown in Fig. 24 for October 2003. Over the Tropics, the MYD08 values are often greater than the CERES values. The opposite is true for the midlatitudes. On average for 2003, D_{eM} is ~2.5 µm greater than D_{eC} in the Tropics and ~3 µm smaller in the midlatitudes. The result is essentially unbiased for nonpolar regions (Table VI). In polar areas, D_{eC} is ~2 µm larger than D_{eM}. Obviously, the spectral differences in the retrievals and the different ice particle models will cause differences in the retrievals. To examine the model and spectral effects, the differences between the CERES and MOD06 D_e(3.8 µm) and D_e(2.1 µm) pixel values were computed using the 3 July 2005 nonpolar Terra granules for phase-matched pixels. The D_{eC} - D_e(2.1 µm) differences were nearly the same as those in Table VI. On average, D_{eC} exceeds D_{eM}(3.8 µm) by 8.9 ± 12.1 µm. This large difference indicates that the MAST ice crystal models yield smaller effective sizes than the CERES models. Since larger values of D_e generally occur lower in the cloud, D_{eM}(2.1 µm) should be greater than D_{eM}(3.8 µm), a relationship that can be inferred here. It is curious that the CERES 3.8-µm retrieval is equivalent to the MAST retrieval for a location lower in the cloud. In Fig. 24, smaller values of D_{eC} tend to occur where small average values of τ_C were found for ice clouds. Thus, the absence of the no-retrieval clouds in the MAST averages probably contributes some to the differences or lack thereof between D_{eC} and D_{eM}. It is not clear why the differences change sign with latitude. Perhaps, there are some systematic differences between the ice crystal habits in the Tropics and midlatitudes.

The values of LWP and IWP are based on the products of cloud optical depth and particle size. Thus, the differences in
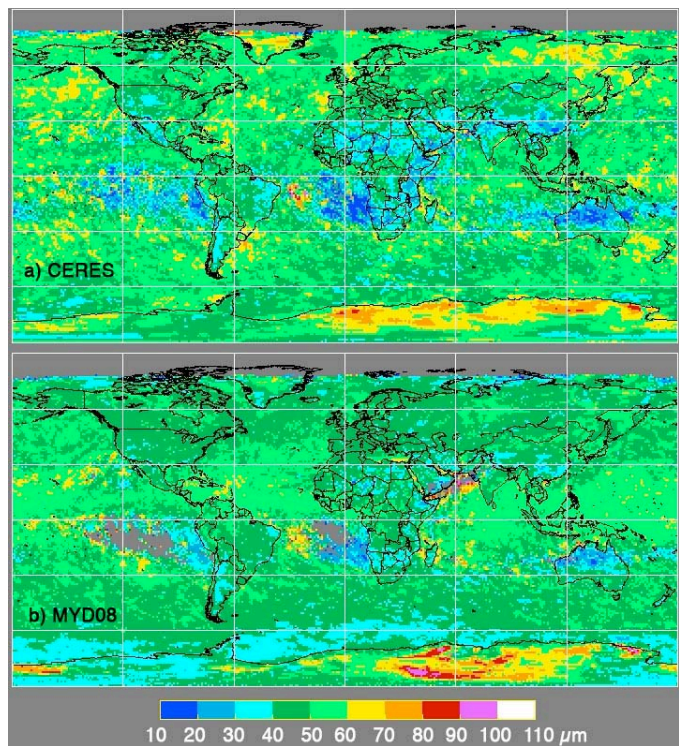
those parameters will transfer into the water path estimates. The mean 2003 differences, LWP_C - LWP_M, are negative everywhere. Over nonpolar regions, the average difference is -29.5 g m^{-2}. This difference is undoubtedly due to the larger values of r_{eM} and the reduced number of optically thin clouds in the MAST averages, as discussed earlier. In polar regions large negative difference is mainly due to the larger optical depths retrieved by the MAST algorithms over snow-covered surfaces. Similar large differences are seen for IWP over the polar regions. However, the nonpolar CERES and MAST IWP values differ by an average of approximately -7.5 g m^{-2}, a difference of only -3.5%. The tropical differences are more strongly negative while those in the midlatitudes are positive, reflecting the differences in D_e noted above.

VI. CONCLUSIONS

As a companion to a detailed description of the methodologies used to retrieve cloud properties for the CERES project, this paper has attempted to provide an overview of retrieved parameters and how they relate to other sources of similar parameters. To that end, it has provided a brief summary of the CERES cloud products derived from VIRS and MODIS data. The quality of and uncertainties in the retrieved properties have been examined using comparisons with independent measurements for a few subsets of the parameters. Differences between the CERES-MODIS properties and those derived from the same dataset using different methods have also been examined.

These analyses lead to the following conclusions.

1) The CERES cloud products are generally consistent quantitatively across the three different satellite platforms.

The greatest discrepancies occur over ice-covered surfaces where different spectral channels were employed and all spectral differences were not taken into account.

2) A day-night change in cloud phase distributions is primarily the result of differences in the day and night retrieval algorithms. The differences are due to different ways of classifying clouds with temperatures in the supercooled cloud range.

3) A day-night change in cloud-top height estimates is also due mostly to algorithm differences. The greater cirrus cloud heights at night are due to the use of infrared channels that are less sensitive to errors in the background temperatures, due to either the presence of low clouds or uncertainties in the surface temperatures.

4) By examining both the CERES-VIRS and CERES-MODIS retrievals, it was found that the mean cloud droplet effective radius undergoes a significant seasonal cycle over the southern hemispheric oceans.

5) Unlike their daytime counterparts, the nighttime cloud microphysical properties are not reliable because of the limitations on cloud optical depth imposed by the availability of only infrared channels. Results for optically thin clouds can be used with caution.

6) Comparisons with surface radar-lidar data and ICESat and CALIPSO lidar measurements indicate that low cloud heights are typically within ± 0.5 km, on average, for a given region outside of the polar zones, where the differences are greater. High-cloud top altitudes are typically underestimated due to inadequate corrections for semi-transparency or the effects of overlapping thin high over low clouds. At night, the optically thin, ice cloud heights are closer to their radar-lidar counterparts. On average over the globe, the CERES clouds are 2.4 km lower than the highly sensitive ICESat GLAS observations. If compared to the weighted average of GLAS-retrieved heights for single-layer clouds and the lowest clouds in multilayered cloud systems, the differences reduces to 0.7 km.

7) For overcast stratus clouds over the ARM SCF, the retrieved values of r_e are, on average, within ±0.2 μm for all three satellite retrievals during the day. The corresponding mean biases in τ vary from -4 to 8%, while those for LWP range from -6 to 14%. A 14% bias relative to ARM MWR measurements of coastal marine stratus was also found. These small positive biases from surface-based measurements contrasts with average underestimates of 28% and 11% over tropical and northern midlatitude oceans from satellite MWR retrievals. Additional study of these discrepancies is needed.

8) Optically thin cirrus optical depths are underestimated by 18 – 40%, on average, during daytime relative to surface-based infrared-radar retrievals, while the VISST-retrieved ice crystal effective sizes differed by -26 to +18%. Mean ice water paths for these same clouds were biased by -16 to +17%. Direct comparisons for thicker ice clouds have not yet been performed, but comparisons of average global IWP with values from CloudSat yield very reasonable results.

9) Regional patterns in average daytime cloud properties from CERES are generally quite similar to those derived using the MODIS Atmosphere Science Team algorithms, but some distinct differences are evident. For the monthly averaged products, the CERES cloud-top pressures are ~69 hPa less than the MAST values indicating the CERES cloud–tops are higher than the MAST clouds. The CERES clouds are lower than the MAST values over the eastern sides of the subtropical highs and parts of the Arctic Ocean. It was found that this difference is due mostly to unretrieved cloudy MAST pixels and pixels having mismatched phases from the two algorithms. If only phase-matched pixels are compared, the mean CERES cloud top pressures are ~45 and 12 hPa greater than the MAST averages for water and ice clouds, respectively.

10) Cloud optical depths are in agreement, on average, for matched CERES and MAST MODIS pixels, where both algorithms retrieve the same phase. When the average products are considered, the mean τ difference between CERES and MAST is roughly -3 and -13 over nonpolar and polar regions, respectively. The difference is primarily due to the absence of many small optical depth clouds, particularly small clouds and cloud edge pixels, in the MAST product. These missing pixels also contribute to the mean IWP and LWP differences between the two products.

11) The monthly averaged CERES cloud droplet sizes are ~2.7-μm smaller than those from MAST because the latter is based on the 2.1-μm radiances and the former is from 3.8-μm radiances which emanate from higher levels within the cloud. On a pixel-level basis, the CERES and MAST 3.8-μm retrievals of r_e are the same, on average, but the average difference between the CERES values and MAST 2.1-μm retrievals is only 1.2 μm. The larger MAST 2.1-μm retrieved droplets sizes suggest that most water clouds are precipitating because the inferred profile has smaller droplets near the cloud top and larger drops near the base. This apparent phenomenon needs further study.

Overall, the CERES cloud products are reasonably accurate despite the observed shortcomings. Much additional validation is required, especially over snow surfaces and thick ice clouds. More detailed comparisons with CloudSat and CALIPSO data will be especially useful in future validation efforts. Additional efforts are needed to better understand the accuracy of the liquid water path retrievals. Future improvements in the algorithms should address many of the known problems including the ozone absorption errors, the thin cirrus optical depth underestimates, and multilayered clouds.

The CERES goal of providing cloud properties coincident with broadband radiation measurements ultimately will require understanding the relationships between cloud properties and the radiation budget. The cloud properties developed for CERES Ed2 are already helping to reconcile

measured and modeled radiative fluxes bringing the theoretical calculations to within 4-6% and -2 to +3 Wm^{-2} of the CERES-measured top-of-atmosphere fluxes [64]. They should prove valuable for many other studies of climate, clouds, and radiation.

REFERENCES

[1] B. A. Wielicki et al., "Clouds and the Earth's Radiant Energy System (CERES): Algorithm overview," *IEEE Trans. Geosci. Remote Sens.*, vol. 36, pp. 1127-1141, 1998.

[2] C. Kummerow, W. Barnes, T. Kozu, J. Shine, and J. Simpson, "The Tropical Rainfall Measuring Mission System (TRMM) sensor package," *J. Atmos. Oceanic Technol.*, vol. 15, pp. 809-827, 1998.

[3] W. L. Barnes, T. S. Pagano, and V. V. Salomonson, "Prelaunch characteristics of the Moderate Resoluiton Imaging Spectroradiometer (MODIS) on EOS-AM1," *IEEE Trans. Geosci. Remote Sens.*, vol. 36, pp. 1088-1100, 1998.

[4] N. G. Loeb, K. J. Priestley, D. P. Kratz, E. B. Geier, R. N. Green, B. A. Wielicki, P. O'R. Hinton, and S. K. Nolan, "Determination of unfiltered radiances from the Clouds and the Earth's Radiant Energy System instrument," *J. Appl. Meteorol.*, vol. 40, pp. 822-835, 2001.

[5] P. Minnis, Q. Z. Trepte, S. Sun-Mack, Y. Chen, D. R. Doelling, D. F. Young, D. A. Spangenberg, W. F. Miller, B. A. Wielicki, R. R. Brown, S. C. Gibson, and E. B. Geier, "Cloud detection in non-polar regions for CERES using TRMM VIRS and Terra and Aqua MODIS data," *IEEE Trans. Geosci. Remote Sens.*, vol. 46, 3857-3884, 2008.

[6] Q. Trepte, P. Minnis, and R. F. Arduini, "Daytime and nighttime polar cloud and snow identification using MODIS data," *Proc. SPIE 3rd Intl. Asia-Pacific Environ. Remote Sensing Symp.,* Hangzhou, China, October 23-27, vol. 4891, 449-459, 2002.

[7] A. Ignatov and L. L. Stowe, "Physical basis, premises, and self-consistency checks of aerosol retrievals from TRMM VIRS," *J. Appl. Meteorol.*, vol. 39, pp. 2259-2277, 2000.

[8] A. Ignatov, A., P. Minnis, N. Loeb, B. Wielicki, W. Miller, S. Sun-Mack, D. Tanre, L. Remer, I. Laszlo, and E. Geier, "Two MODIS aerosol products over ocean on the Terra and Aqua CERES SSF datasets," *J. Atmos Sci.*, 62, pp.1008-1031, 2005.

[9] P. Minnis, S. Sun-Mack, D. F. Young, P. W. Heck, D. P. Garber, Y. Chen, D. A. Spangenberg, R. F. Arduini, Q. Z. Trepte, W. L.Smith, Jr., J. K. Ayers, S. C. Gibson, W. F. Miller, V. Chakrapani, Y. Takano, K.-N. Liou, and Y. Xie, "CERES Edition 2 cloud property retrievals using TRMM VIRS and Terra and Aqua MODIS data: Part I: Algorithms," *IEEE Trans. Geosci. Remote Sens.*, same issue, 2011.

[10] S. A. Ackerman, K. I. Strabala, W. P. Menzel, R. A. Frey, C. C. Moeller, and L. E. Gumley, "Discriminating clear sky from clouds with MODIS," *J. Geophys. Res.*, vol. 103, pp. 32 141–32 157, 1998.

[11] M. D. King et al., "Cloud and aerosol properties, precipitable, water, and profiles of temperature and water vapor," *IEEE Trans. Geosci. Remote Sens.*, vol. 41, pp. 442-458, 2003.

[12] S. Platnick, M. D. King, S. A. Ackerman, W. P. Menzel, B. A. Baum, J. C. Riedl, and R. A. Frey, "The MODIS cloud products: Algorithms and examples from Terra," *IEEE Trans. Geosci. Remote Sens.*, vol. 41, pp. 459-473, 2003.

[13] M. D. King, S. Platnick, P. A. Hubanks, G. T. Arnold, E. G. Moody, G. Wind and B. Wind. (2006). *Collection 005 Change Summary for the MODIS Cloud Optical Property (06_OD) Algorithm*. [Online]. Available: modis-atmos.gsfc.nasa.gov/C005_Changes/C005_CloudOpticalProperties_ver311.pdf

[14] W. P. Menzel, et al., "MODIS cloud-top pressure and amount estimation: Algorithm description and results.," *J. Appl. Meteorol. Clim.*, vol. 47, pp. 1175-1198, 2008.

[15] R. A. Frey, S. A. Ackerman, Y. Liu, K. I. Strabal, H. Zhang, J. R. Key, and X. Wang, "Cloud detection with MODIS. Part I: Improvements in the MODIS cloud mask for Collection 5," ," *J. Atmos. Oceanic Technol.*, vol. 25, pp. 1057-1072, 2008.

[16] Wentz, F. and T. Meissner, "AMSR Ocean Algorithm, Algorithm Theoretical Basis Document, Version 2," *RSS Tech Rpt. 121599A-1*, Santa Rosa, CA, USA: Remote Sensing Systems, 66 pp., 2000.

[17] B. Lin, P. Minnis, B. A. Wielicki, D. R. Doelling, R. Palikonda, D. F. Young, and T. Uttal, "Estimation of water cloud properties from satellite microwave and optical measurements in oceanic environments. II: Results," *J. Geophys. Res.*, vol. 103, 3887-3905, 1998.

[18] J. Huang, P. Minnis, B. Lin, Y. Yi, T.-F. Fan, S. Sun-Mack, and J. K. Ayers, "Determination of ice water path in ice-over-water cloud systems using combined MODIS and AMSR-E measurements," *Geophys. Res. Lett.*, vol. 33, L21801, 10.1029/2006GL027038, 2006.

[19] J. D. Spinhirne, S. P. Palm, W. D. Hart, D. L. Hlavka, and E. J. Welton, "Cloud and aerosol measurements from GLAS: Overview and initial results," *Geophys. Res. Lett.*, vol. 32, L22S03, doi: 10.1029/2005GL023507, 2005.

[20] T. P. Ackerman and G. P. Stokes, "The Atmospheric Radiation Measurement Program," *Phys. Today*, vol. 56, pp. 38-44, 2003.

[21] M. A. Miller, A. Bucholtz, B. Albrecht, and P. Kollias. (2005). *Marine Stratus Radiation, Aerosol, and Drizzle (MASRAD) science plan*. [Online]. Available: http://www.arm.gov/publications/programdocs/doe-er-arm-0501.pdf

[22] G. G. Mace, S. Benson, K. L. Sonntag, S. Kato, Q. Min, P. Minnis, C. H. Twohy, M. Poellot, X. Dong, C. Long, Q. Zhang, and D. R. Doelling, "Cloud radiative forcing at the ARM climate research facility: Part I. Technique, validation, and comparison to satellite-derived quantities," *J. Geophys. Res.*, vol. 111, 10.1029/2005JD005921, 2006.

[23] J. C. Liljegren, E. E. Chlotiaux, G. G. Mace,S. Kato, and X. Dong, "A new retrieval for cloud liquid water path using a ground-based microwave radiometer and measurements of cloud temperature," J. Geophys. Res., vol. 103, pp. 23,207-23,216, 2001.

[24] X. Dong, P. Minnis, B. Xi, S. Sun-Mack, and Y. Chen, "Comparison of CERES-MODIS stratus cloud properties with ground-based measurements at the DOE ARM Southern Great Plains site," *J. Geophys. Res.*, vol. 113, D03204, doi:10.1029/2007JD008438, 2008.

[25] G. G. Mace, T. P. Ackerman, P. Minnis, and D. F. Young, "Cirrus layer microphysical properties derived from surface-based millimeter radar and infrared interferometer data," *J. Geophys. Res.*, vol. 103, pp. 23,207-23,216, 1998.

[26] G. G. Mace, Y. Zhang, S. Platnick, M. D. King, P. Minnis, and P. Yang, "Evaluation of cirrus cloud properties from MODIS radiances using cloud properties derived from ground-based data collected at the ARM SGP site," *J. Appl. Meteorol.*, vol. 44, pp. 221-240, 2005.

[27] D. Waliser, et al., "Cloud ice: A climate model challenge with signs and expectations of progress," *J. Geophys. Res.*, vol. 114, D00A21, doi:10.1029/2008JD010015, 2009.

[28] P. Minnis, D. R. Doelling, L. Nguyen, W. F. Miller, and V. Chakrapani, "Assessment of the visible channel calibrations of the TRMM VIRS and MODIS on *Aqua* and *Terra*," J. Atmos. Oceanic Technol., vol. 25, pp. 385-400, 2008.

[29] W. L. Smith, P. Minnis, H. Finney, R. Palikonda, and M. M. Khaiyer, "An evaluation of operational GOES-derived single-layer cloud top heights with ARSCL over the ARM Southern Great Plains site,"

Geophys. Res. Lett., vol. 35, L13820, doi:10.1029/2008GL034275, 2008.

[30] S. Sun-Mack, B. A. Wielicki, P. Minnis, S. Gibson, and Y. Chen, "Integrated cloud-aerosol-radiation product using CERES, MODIS, CALISPO, and CloudSat data," *Proc. SPIE Europe 2007 Conf. Remote Sens. Clouds and the Atmos.*, Florence, Italy, 17-19 September, vol. 6745, no. 29, 11 pp., 2007.

[31] S. C. Sherwood, J.-H. Chae, P. Minnis, and M. McGill,"Underestimation of deep convective cloud tops by thermal imagery," *Geophys. Res. Lett.*, vol. 31, 10.1029/2004GL019699, 2004.

[32] P. Minnis, C. R. Yost, S. Sun-Mack, and Y. Chen, "Estimating the physical top altitude of optically thick ice clouds from thermal infrared satellite observations using CALIPSO data," *Geophys. Res. Lett.*, vol. 35, L12801, doi:10.1029/2008GL033947, 2008.

[33] P. Minnis, D. P. Garber, D. F. Young, R. F. Arduini, and Y. Takano, "Parameterization of reflectance and effective emittance for satellite remote sensing of cloud properties," *J. Atmos. Sci.*, vol. 55, pp. 3313-3339, 1998.

[34] B. Xi, X. Dong, P. Minnis, and M. M. Khaiyer, "A 10-year climatology of cloud cover and vertical distribution derived from both surface and GOES observations over the DOE ARM SGP site", *J. Geophys. Res.*, vol. 115, D12124, doi:10.1029/2009JD012800, 2010.

[35] P. Minnis and E. F. Harrison, "Diurnal variability of regional cloud and clear-sky radiative parameters derived from GOES data, Part II: November 1978 cloud distributions," *J. Clim. Appl. Meteorol.*, vol. 23, pp. 1012-1031, 1984.

[36] C. M. Alcala and A. E. Dessler, "Observations of deep convection in the tropics using the Tropical Rainfall Measuring Mission (TRMM) precipitation radar," *J. Geophys. Res.*, vol.. 107, doi:10.1029/2002JD002457, 2002.

[37] C. Liu and E. J. Zipser, "Global distribution of convection penetrating the tropical tropopause," *J. Geophys. Res.*, vol. 110, doi:10.1029/2005JD006063, 2005.

[38] C. Liu, E. J. Zipser, G. G. Mace, and S. Benson, "Implications of the differences between daytime and nighttime CloudSat observations over the tropics," J. Geophys. Res., vol. 113, doi:10.1029/2008JD009783, 2008.

[39] X. Dong, P. Minnis, G. G. Mace, W. L. Smith, Jr., M. Poellot, R. T. Marchand, and A. D. Rapp, "Comparison of stratus cloud properties deduced from surface, GOES, and aircraft data during the March 2000 ARM Cloud IOP," *J. Atmos. Sci.*, vol. 59, pp. 3256-3284, 2002.

[40] D. D. Turner, et al., "Thin liquid water clouds: Their importance and our challenge," *Bull. Am. Meteorol. Soc.*, vol. 88, pp. 177-190, 2007.

[41] X. Dong, G. G. Mace, P. Minnis, and D. F. Young, "Arctic stratus cloud properties and their impact on the surface radiation budget; Selected cases from FIRE ACE," *J. Geophys. Res.*, vol. 106, pp. 15,297-15,312, 2001.

[42] P. Minnis, P., D. F. Young, B. A. Weilicki, S. Sun-Mack, Q. Z. Trepte, Y. Chen, P. W. Heck, and X. Dong, "A global cloud database from VIRS and MODIS for CERES," *Proc. SPIE 3rd Intl. Asia-Pacific Environ. Remote Sensing Symp. 2002: Remote Sens. of Atmosphere, Ocean, Environment, and Space*, Hangzhou, China, October 23-27, vol. 4891, pp. 115-126, 2003.

[43] T. J. Greenwald, T. S. L'Ecuyer, and S. A. Christopher, "Evaluating specific error characteristics of microwave-derived liquid water paths," *Geophys. Res. Lett.*, vol. 34, L22807, doi:10.1029/2007GL031180, 2007.

[44] F.-L. Chang and Z. Li, "Estimating the vertical variation of cloud droplet effective radius using multispectral near-infrared satellite measurements," *J. Geophys. Res.*, vol. 107, 4257, doi:10.1029/2001JD000766, 2002.

[45] F.-L. Chang and Z. Li, "Retrieving vertical profiles of cloud droplet effective radius: Algorithm modification and preliminary application," *J. Geophys. Res.*, vol. 108, 4763, doi:10.1029/2003JD003906, 2003.

[46] R. Chen, F.-L. Chang, Z. Li, R. Ferraro, and F. Weng, " Impact of the vertical variation of cloud droplet size on the estimate ofliquid water path and rain detection," *J. Atmos. Sci.*, vol. 64, pp. 3843-3853, 2007.

[47] R. Chen, R. Wood, Z. Li, R. Ferraro, and F.-L. Chang," Studying the vertical variation of cloud droplet effective radius using ship and space-borne remote sensing data," *J. Geophys. Res.*, vol. 113, D00A02, doi:10.1029/2007JD009596, 2008.

[48] C. Seethala and A. Horvath, " Global assessment of AMSR-E and MODIS cloud liquid water path retrievals in warm oceanic clouds," *J. Geophys. Res.*, vol. 115, doi: 10.1029/2009JD012662, 2010.

[49] Q. Min, P. Minnis, and M. M. Khaiyer, "Comparison of cirrus optical depths from GOES-8 and surface measurements," *J. Geophys. Res.*, vol. 109, D20119, 10.1029/2003JD004390, 2004.

[50] J. M. Comstock, R. d'Entremont, D. DeSlover, G. G. Mace, S. Y. Matrosov, S. A. McFarlane, P. Minnis, D. Mitchell, K. Sassen, M. D. Shupe, D. D. Turner, and Z. Wang, "An intercomparison of microphysical retrieval algorithms for upper tropospheric ice clouds," *Bull. Am. Meteorol. Soc.*, vol. 88, pp. 191-204, 2007.

[51] P. Yang, P., G. W. Kattawar, G. Hong, P. Minnis, and Y. X. Hu, "Uncertainties associated with the surface texture of ice particles in satellite-based retrieval of cirrus clouds: Part II. Effect of particle surface roughness on retrieved cloud optical thickness and effective particle size," *IEEE Trans. Geosci. Remote Sens.*, vol. 46(7), 1948-1957, doi:10.1109/TGRS.2008.916472, 2008.

[52] Y. Xie, P. Yang, G. W. Kattawar, P. Minnis, and Y. Hu, "Effect of inhomogeneity of ice crystals on retrieving ice cloud optical thickness and particle size," *J. Geophys. Res.*, vol. 114, D11203, doi:10.1029/2008JD011216, 2009.

[53] P. Yang, L. Zhang, G. Hong, S. L. Nasiri, B. A. Baum, H. L. Huang, M. D. King, and S. Platnick, "Differences between collection 4 and 5 MODIS ice cloud optical/microphysical products and their impact on radiative forcing simulations," *IEEE Transactions on Geoscience and Remote Sensing*, vol. 45(9), pp. 2886-2899, 2007.

[54] P. Minnis, J. Huang, B. Lin, Y. Yi, R. F. Arduini, T.-F. Fan, J. K. Ayers, and G. G. Mace, "Ice cloud properties in ice-over-water cloud systems using TRMM VIRS and TMI data," *J. Geophys. Res.*, vol. 112, D06206, doi:10.1029/2006JD007626, 2007.

[55] W. B. Rossow and R. A. Schiffer, "Advances in understanding clouds from ISCCP," *Bull Am. Meteor. Soc.*, vol. 80, pp. 2261-2287, 1999.

[56] S. M. Thomas, A. K. Heidinger, and M. J. Pavolonis, "Comparison of NOAA's operational AVHRR-derived cloud amount to other satellite-derived cloud climatologies," *J. Climate*, vol. 17, pp. 4805-4822, 2006.

[57] Wylie, D. P., D. L. Jackson, W. P. Menzel, and J. J. Bates, 2005: Trends in Global Cloud Cover in two Decades of HIRS Observations, J. Climate 18, 3021-3031.

[58] Stubenrauch, C. J., Chédin, A., Rädel, G., Scott, N. A., Serrar, S., 2006a: Cloud properties and their seasonal and diurnal variability from TOVS Path-B. J. Climate 19, 5531-5553.

[59] R. E. Holz, S. A. Ackerman, F. W. Nagle, R. Frey, S. Dutcher, R. E. Kuehn, M. A. Vaughan, and B. Baum, "Global Moderate Resolution Imaging Spectroradiometer (MODIS) cloud detection and height evaluation using CALIOP," *J. Geophys. Res.*, vol. 113, D00A19, doi:10.1029/2008JD009837, 2008.

[60] B. A. Baum, P. Yang, A. J. Heymsfield, S. Platnick, M. D. King, Y.-X. Hu, and S. T. Bedka, "Bulk scattering properties for the remote sensing of ice clouds. Part II: Narrowband models," *J. Appl. Meteorol.*, vol. 44, 1896-1911, 2005.

[61] M. D. King, S. C. Tsay, S. E. Platnick, M. Wang, and K. N. Liou, "Cloud retrieval algorithms for MODIS: Optical thickness, effective particle radius, and thermodynamic phase," *MODIS Algorithm Theoretical Basis Document No. ATBD-MOD-05*, 79 pp., 1997. [Online]. Available: modis-atmos.gsfc.nasa.gov/_docs/atbd_mod05.pdf

[62] M. D. King, S. Platnick, P. A. Hubanks, G. T. Arnold, E. G. Moody, G. Wind and B. Wind,*Collection 005 Change Summary for the MODIS Cloud Optical Property (06_OD) Algorithm*, 2006. [Online]. Available: modis-atmos.gsfc.nasa.gov/C005_Changes/C005_CloudOpticalProperties_ver311.pdf

[63] M. Chiriaco, H. Chepfer, P. Minnis, M. Haeffelin, S. Platnick, D. Baumgardner, P. Dubuisson, M. McGill, V. Noel, J. Pelon, D. Spangenberg, S. Sun-Mack, and G. Wind, "Comparison of CALIPSO-like, LaRC, and MODIS retrievals of ice cloud properties over SIRTA in France and Florida during CRYSTAL-FACE," *J. Appl. Meteorol. Climatol.*, vol. 46, pp. 249-272, 2007.

[64] T. P. Charlock, F. G. Rose, D. A. Rutan, Z. Jin, S. Kato, W. Su, L. Coleman, T. E. Caldwell, D. Fillmore, and W. D. Collins, "Surface and Atmosphere Radiation Budget (SARB) Report," Presented at 8th CERES-II Sci. Team Mtg., Victoria, BC, Canada, 14-16 November, 23 pp., 2007. [Online]. Available: http://science.larc.nasa.gov/ceres/STM/2007-11/ce0711141635Charlock.pdf

[65] W. Hunt, D. M. Winker, M. A. Vaughan, K. A. Powell, P. L. Lucker, and C. Weimer, "CALIPSO lidar description and performance assessment," J. Atmos. Oceanic Technol., vol. 26, pp. 1214-1228, 2009.

[66] T. Y. Nakajima, K. Suzuki, and G. L. Stephens, "Droplet growth in warm water clouds observed by the A-Train: sensitivity analysis of the MODIS-derived cloud droplet sizes," J. Atmos., Sci., vol. 67, pp. 1884-1896, 2010.

[67] K. Suzuki, T. Y. Nakajima, and G. L. Stephens, "Particle growth and drop collection efficiency of warm clouds as inferred from joint CloudSat and MODIS observations," J. Atmos., Sci., vol. 67, pp. 3019-3032, 2010.

Patrick Minnis, a native of Oklahoma City, received the B.E. degree in materials science and metallurgical engineering from Vanderbilt University, Nashville, TN, in 1972, the M.S. degree in atmospheric science from Colorado State University, Fort Collins, in 1978, and the Ph.D. degree in meteorology from the University of Utah, Salt Lake City, in1991.

He is currently a Senior Research Scientist with the Climate Sciences Branch, NASA Langley Research Center, Hampton, VA, where he has served for more than 33 years. His research is focused on the remote sensing of clouds and surface properties from satellite imagery for weather and climate investigations. He is the author/coauthor of over 200 peer-reviewed publications. He is a member of the CERES, ARM, CALIPSO, and ACCRI Science Teams and leads a research group conducting analyses of polar-orbiting and geostationary satellite data for field missions, aircraft safety, and weather and climate research.

Dr. Minnis is a fellow of the American Geophysical Union and American Meteorological Society, and a member of the AIAA. He was the recipient of NASA medals for Exceptional Scientific Achievement in1993, Exceptional Achievement in 2005, and Exceptional Service in 2008, and the AMS Henry G. Houghton Award for Atmospheric Physics in 1998 and the 2011 AIAA Losey Atmospheric Sciences Award.

Szedung (Sunny) Sun-Mack received the B.S degree in Astrophysics from Peking University, Beijing China, the M.S. Degree in Physics from University of Maryland, Maryland, and the Ph.D degree in Physics from Simon Fraser University/TRIUMF (Tri-Universities Meson Facility), Vancouver, British Columbia, Canada in 1994.

She jointed the CERES team, National Aeronautics and Space Administration (NASA) Langley Research Center (LaRC), through various contract companies (Lockheed, SAIC and SSAI) in 1993, and has worked on many projects like A-Train and NPP as well as CERES from 1995 to 2008.

Prior to that, she held a research position at TRIUMF, Canada's National Laboratory for Particle and Nuclear Physics, for 3 years and at Beijing Astronomical Observatory, China Academia Sinica for 2 years. Her research experience includes cloud and surface remote sensing, validation, integration of cloud properties from MODIS, CALIPSO and CloudSat, and developing and operating large complex end-to-end processing systems.


Yan Chen received a B.S. in mechanical engineering from Shanghai Jiao Tong University, China in 1984, and a M.S. in mechanical engineering from the University of Alabama in Huntsville in 1992.

She has been working for Science Systems and Applications, Inc. to support the NASA CERES, NEWS, and NPP projects since Dec. 2006. Previously, she worked for Science Applications International Corporation to support CERES project. She has more than ten years of experience in satellite data analysis by working with CERES Clouds Working group to develop surface emissivity maps, clear sky overhead albedo maps and algorithm analysis software.

Mandana Khaiyer received the M.S. degree in meteorology from The Pennsylvania State University, State College, PA, in 1997. She is currently a Senior Research Scientist at Science Systems and Applications, Inc, in Hampton, VA. She has 13 years of experience providing support and validation of satellite retrieval algorithms, for various projects including CERES.

Yuhong (Helen) Yi received the B.S. degree in meteorology from Nanjing Institute of Meteorology, Nanjing, China, in 1984, the M.S. degree in atmospheric science from Lanzhou Institute of Atmospheric Physics of Chinese Academy, China, in 1987, and the Ph. D. degree in climate change and modeling from Texas A&M University, College Station, in 1996.

She is currently a Senior Research Scientist with Science Systems and Applications, Inc., Hampton, VA. Prior to that, she was with the Analytical Services and Materials, Inc. as a contract scientist of NASA Langley Research Center through the Analytical Services and Materials, Inc., Hampton, VA. She has been involved in the various projects, such as CERES, CALIPSO and CloudSat, and has extensive experience in satellite cloud property retrieval and validation.
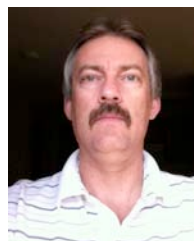
J. Kirk Ayers, a native of Phil Campbell, Alabama, received the B. S. degree in chemical engineering from the University of Alabama in 1985.

He is currently a Senior Research Scientist with Science Systems and Applications Incorporated in Hampton, Virginia. He has 25 years experience in mathematical modeling, satellite data analysis, and development of computer software for analysis of scientific and engineering problems. For the past 16 years he has supported the NASA Langley Research Center Climate Sciences Branch and coauthored more than 25 peer-reviewed publications. His research interests are derivation and validation of remotely sensed cloud properties, and the investigation of the effects of anthropogenic aerosols on atmospheric radiation and climate.

Ricky Brown started working for NASA Langley Research Center in 1997 as part of the CERES Clouds Working Group and Data Management Team as a Programmer Analyst. He has also worked with the CERES Instrument Subsystem. He has served on the CERES team for the past 14 years. Ricky received a Bachelor of Science degree in Computer Science from Christopher Newport University, Newport News, Virginia, in 1998.

Xiquan Dong received the Ph.D degree in Meteorology from the Pennsylvania State University, State College, in 1996.

He is currently professor in the Department of Atmospheric Sciences, the University of North Dakota, Grand Forks. He was research scientist for NASA Langley Research Center through AS&M Company, and an assistant research professor at University of Utah before he joined in the University of North Dakota in 2002. His research interests include the ground- and satellite-based remote sensing, clouds and radiation, and climate changes and extremes.

Sharon Gibson has been working with the NASA CERES project since it's inception. She holds an undergraduate degree from California Polytechnic State University, San Luis Obispo, and a M.S degree in Imaging Science from Rochester Institute of Technology, Rochester, NY, with a research focus in remote sensing and digital image/signal processing. She has primary responsibility for the software development, testing and utilization of data analysis and visualization tools used for validation of cloud retrieval and other science algorithms.

She focuses primarily on the development of tools that are both convenient for use by the individual scientist and helpful for expediting the large scale processing of hybrid data sets necessary for more extensive, long term topical studies. Over the years, she has also contributed to the NASA's DIAL and HALOE programs. She is currently with Science Systems and Applications, Inc., Hampton, VA.

Patrick Heck received a B.S. degree in meteorology from Iowa State University (ISU), Ames, IA, in 1983 and attended graduate school at ISU. He worked until 2003 with contractors in the Science Directorate at NASA Langley Research Center, Hampton, VA, and is currently a Researcher at the Cooperative Institute for Meteorological Satellite Studies at University of Wisconsin-Madison, Madison, WI. His research focuses on the development of algorithms for the retrieval of cloud macro- and microphysical properties from satellite data.

Bing Lin is a senior research scientist in the Science Directorate of the NASA Langley Research Center, Hampton, Virginia, USA. He received his M.S. (1992) and Ph.D. (1995) degrees in Atmospheric Sciences from Columbia University, New York. Dr. Lin also obtained his B. Eng. (1983) and M. Eng. (1986) degrees in Electrical Engineering from the University of Science and Technology of China and the Institute of Electronics of the Chinese Academy of Sciences, respectively. Dr. Lin has worked on satellite remote sensing for more than 15 years and authored/co-authored over 50 peer-reviewed journal articles. His research interests include atmospheric radiation, cloud and climate feedbacks, remote sensing of atmosphere, land and ocean, radiative transfer theory, and the Earth's water and energy cycle.

Michele Nordeen received the B. S. degree in meteorology from Iowa State University, Ames, in 1997, and the M. S. degree in Atmospheric Science from Texas A&M University, College Station, in 2000.

She has been with the NASA Langley Research Center, Hampton, VA, since 1999, through contracts with Analytical Services and Materials, Inc, and Science Systems and Applications, Inc., where she currently supports the CERES and ARM projects through data analysis and validation.

Louis Nguyen received a B.S. degree in computer science from Old Dominion University, Norfolk, VA, in 1994, and a M.S. Degree in computer science from Old Dominion University in 2011.

He began his professional career in 1994 and has 17 years of experience working in the field of atmospheric science research. He is currently working as a Research Computer Engineer in the Climate Science Branch of the Science Directorate (SD) at NASA Langley Research Center, Hampton VA. His research area focused on the computer systems, algorithms, and software for conducting remote sensing and climate science research. He is author/coauthor of over 17 peer-reviewed publications and over 60 referenceable conference papers. He is a member of the Clouds and the Earth's Radiant Energy System (CERES) Science Team and is currently a Ph. D. candidate at Old Dominion University Computer Science Department.

Mr. Nguyen was the recipient of NASA Superior Accomplishment Award in 2002, 2003, and 2004, the NASA Exceptional Achievement Medal in 2003, and the Paul F. Holloway Non-Aerospace Technology Transfer Award in 2007.

Rabindra Palikonda received the B.E. degree in metallurgy from PSG College of Engineering, Coimbatore, India in 1987, the M.S. degree in computer science from South Dakota School of Mines & Technology, Rapid City, SD, in 1992.

He has worked at NASA Langley Research Center, Hampton, VA, since 1992, through contracts with Lockheed Engineering & Sciences, Co., Analytical Services & Materials, Inc. and Science Systems & Applications, Inc. His work is focused on developing scientific algorithms and computer software for analysis of remotely sensed satellite data for various projects including the CERES project. He has primary responsibility for adapting the MODIS-based CERES cloud retrieval software to use on geostationary satellite data in support of TISA, nowcasting and global NWP model assimilation projects. Mr. Palikonda was awarded the NASA 2007 Paul F. Holloway Non-Aerospace Technology Transfer Award for his work on the real-time icing diagnosis product.

William L. Smith Jr. received the B.S. degree in Meteorology from the University of Wisconsin-Madison and the M.S. in Atmospheric Science from Colorado State University in 1989. In 1990, he came to NASA Langley Research Center in Hampton, VA, where he is currently a Research Scientist in the Science Directorates' Chemistry and Dynamics Branch. His research interests include the passive remote sensing of cloud and radiation parameters from satellites for weather and climate applications, and associated verification activities using active remote sensing and other data obtained from ground-based, aircraft and satellite platforms.
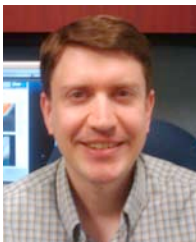
Douglas Spangenberg received the B.S. and M.S. degrees in meteorology from The Pennsylvania State University, University Park, PA in 1993 and 1995, respectively.

He has been working at NASA-Langley Research Center in Hampton, VA since 1997 through contracts with Analytical Services & Materials, Inc. and more recently, Science Systems & Applications, Inc. His primary work is focused on supporting the CERES project. He has extensive experience in the satellite cloud property retrieval validation effort and has developed algorithms for the display, analysis and calibration of data from geostationary and polar orbiting satellites using the Man Computer Interactive Data Access System (McIDAS). His research interests include studying polar cloud systems using Terra and Aqua MODIS data and using satellite data to determine the risk of ice buildup on aircraft flying through clouds. Mr. Spangenberg is a member of the American Meteorological Society.

Qing Trepte received a B.S. degree in Atmospheric Physics from Nanjing University, Nanjing, China in 1983 and a M.S. degree in Meteorology from the University of Wisconsin-Madison in 1990. She is currently an atmospheric scientist with Science Systems & Applications, Inc. (SSAI) in Hampton, VA and is a member of the NASA Langley CERES cloud retrieval team. Her primary responsibilities are developing, testing, and validating algorithm improvements to the daytime, nighttime, and twilight CERES cloud masks for polar and non-polar regions using MODIS, GOES, MSG, MTSAT, and AVHRR satellite data.

Baike Xi received the Ph.D degree in Meteorology from the Pennsylvania State University, State College, in 1999.

She is currently an associate research professor in the Department of Atmospheric Sciences, the University of North Dakota, Grand Forks. She was a Postdoctoral Researcher at the University of Utah before she joined in the University of North Dakota in 2003. Her research interests include the aerosol physical and chemical properties, ground- and satellite-based remote sensing, and clouds and radiation.